# Method to study relaxation of metastable phases: Macroscopic mean-field dynamics

Jooyoung Lee,[1,*] M. A. Novotny,[1,†] and Per Arne Rikvold[1,2,‡]
[1] *Supercomputer Computations Research Institute, Florida State University, Tallahassee, Florida 32306-4052*
[2] *Center for Materials Research and Technology and Department of Physics, Florida State University, Tallahassee, Florida 32306-3016*
(Received 9 March 1995)

We propose two different macroscopic dynamics to describe the decay of metastable phases in many-particle systems with local interactions. These dynamics depend on the macroscopic order parameter $m$ through the restricted free energy $F(m)$ and are designed to give the correct equilibrium distribution for $m$. The connection between macroscopic dynamics and the underlying microscopic dynamic is considered in the context of a projection-operator formalism. Application to the square-lattice nearest-neighbor Ising ferromagnet gives good agreement with droplet theory and Monte Carlo simulations of the underlying microscopic dynamic. This includes quantitative agreement for the exponential dependence of the lifetime $\langle\tau\rangle$ on the inverse of the applied field $H$, and the observation of distinct field regions in which $\Lambda \equiv d\ln\langle\tau\rangle/d|H|^{1-d}$ depends differently on $|H|$. In addition, at very low temperatures we observe oscillatory behavior of $\Lambda$ with respect to $|H|$, which is due to the discreteness of the lattice and in agreement with rigorous results. Similarities and differences between this work and earlier works on finite Ising models in the fixed-magnetization ensemble are discussed.

PACS number(s): 64.60.My, 64.60.Qb, 02.70.Lq, 05.50.+q

## I. INTRODUCTION

Metastable phases are observed in a wide variety of systems that exhibit first-order phase transitions. A few examples are supercooled fluids, permanent magnets, ferroelectrics, and certain alloys. In high-energy physics and cosmology, the existence of metastable phases has also been discussed, such as the "false vacuum" associated with the electroweak phase transition, and the supercooled quark-gluon plasma associated with the QCD confinement transition. In recent decades, much attention has been focused on the study of metastable phases and the rate at which they decay to thermodynamic equilibrium, but a fully satisfactory description has remained elusive. A recent review with numerous references to specific realizations of metastable behavior in real and model systems is found in Ref. [1].

In certain systems with weak long-range interactions, infinitely long-lived metastable phases can exist in the thermodynamic limit [2]. However, in systems with short-range interactions, there exist no such stable non-equilibrium states, even in the thermodynamic limit. Nevertheless, for large but finite systems, the relaxation time for short-range models can be extremely long compared with any finite observation time [3–6]. Here, we define the term "metastability" to include this phenomenon in short-range models. The long relaxation time is mainly due to the large free energy of the local fluctuations that must spontaneously arise in order for the system to decay into a globally stable phase. Due to the long relaxation time, it is difficult to tell metastable phases from globally stable ones by observing only short-time fluctuations. The explorations of phase space, characteristic of the metastable phase, are expected to be those included in a constrained partition function that excludes the microstates that dominate in equilibrium [2,7]. The application of such ideas to a field-theoretical droplet model with Fokker-Planck dynamics has shown that close to coexistence, the nucleation rate for droplets of the equilibrium phase is proportional to the imaginary part of a complex-valued constrained free energy obtained by analytic continuation from the equilibrium phase into the metastable phase [8–10].

Recently, complex-valued constrained free energies were numerically obtained for both the two-dimensional nearest-neighbor Ising ferromagnet [11,12] and for models with weak long-range forces [13–15] by a constrained-transfer-matrix method introduced by one of us [16]. Although no dynamical aspects were explicitly considered to obtain the constrained free energies, the average free-energy cost of a critical droplet was obtained over a wide range of fields and temperatures, in good agreement with the predictions of field-theoretical droplet models [8–10,14,15,17] and Monte Carlo (MC) simulations [1,4–6]. These results indicate the relevance of purely static properties, such as the free energy, to the relaxation behavior of metastable phases. Whereas any physical dynamic (consistent with a real experimental situation) is bound to give the correct *equilibrium* Boltzmann distribution for an infinitely long observation time, it is not yet clear how relevant the static properties of a model are to the study of the dynamical relaxation of a metastable

*Present address: Baker Laboratory of Chemistry, Cornell University, Ithaca, NY 14853-1301. Electronic address: jlee@scheraga2.tn.cornell.edu
†Electronic address: novotny@scri.fsu.edu
‡Electronic address: rikvold@scri.fsu.edu

 

phase towards equilibrium.

The observations discussed in the preceding paragraph raise the interesting possibility that the information stored in static quantities may be sufficient to describe the salient features of the relaxation behavior of a metastable phase, even in a short-range-force system. A quantity that contains all thermodynamically relevant equilibrium information is the restricted bulk free energy,

$$F(m) = F_0(m) - \beta H N m \,, \tag{1}$$

where $m$ is the macroscopic order parameter conjugate to the external field $H$. Here $\beta=1/T$ is the inverse temperature with Boltzmann's constant $k_B=1$, and $\beta$ has been absorbed in $F(m)$ and $F_0(m)$. One can obtain $F(m)$ either exactly from exact enumerations for small systems, or approximately, up to an additive constant, by Monte Carlo simulation. The importance of the detailed shape of the zero-field free energy $F_0(m)$ for two-phase equilibria and nucleation barriers has previously been discussed by Schulman [3] and Binder and co-workers [18–20]. Generalizations of Eq. (1) to consider several macroscopic densities and their conjugate fields are straightforward.

Since the restricted bulk free energy is (by definition) projected onto a space spanned by one or a small number of macroscopic densities, all detailed information about microscopic spin configurations is lost. In this paper, we investigate the possibility that macroscopic dynamical properties that are common to several different microscopic dynamics may, nevertheless, be extracted from the information retained in $F(m)$. For this purpose, we construct two different macroscopic, discrete-time dynamics, each defined by a separate master equation for the order-parameter distribution function. Both master equations are subject to the following two restrictions.

(1) The order parameter $m$ is allowed to change only by a finite amount during each discrete time step (locality in $m$).

(2) The dynamics should reproduce the correct $F(m)$ in equilibrium [correct static properties of $F(m)$].

Although the relevance to metastable decay of the Hohenberg-Halperin scheme of dynamic universality classes [21] is not completely clear, we demonstrate in this work that the requirements (1) and (2) are sufficient to make our macroscopic dynamics consistent with microscopic dynamics in the class of Model A: systems with a nonconserved scalar order parameter and local dynamic.

For short-range-force models, the sequence of microscopic configurations that constitutes a particular realization of a MC simulation cannot be deduced from the corresponding sequence of values of macroscopic variables. In contrast, for models in which each site interacts equally with all other sites while the total interaction energy remains independent of the system size (equivalent-neighbor models), all configurations with identical values of the order parameter are equivalent, so the dynamical properties can be exactly obtained from the restricted free energy, as has been shown by Griffiths *et al.* [22]. In the equivalent-neighbor limit, one of the macroscopic dynamics that we propose in this work reduces to the Metropolis [23] version of the heat-bath dynamic studied in Ref. [22]. (For discussions of the distinctions between Metropolis and heat-bath or Glauber dynamics, see, e.g., Refs. [1,24].) Since it is well known that both the equilibrium and the metastable properties of equivalent-neighbor models are exactly described by mean-field theory in the thermodynamic limit [2,13–15], these models are often referred to as "mean-field models" [22]. Consistent with this usage, we call the class of dynamics that we define here "macroscopic mean-field dynamics."

Our proposed dynamics may be considered as approximations to the dynamic one would obtain by projecting the microscopic dynamic onto a master equation for the macroscopic order-parameter distribution [3], using a projection-operator technique [25–30]. This point of view is further explored in Appendix A. Since the decay of metastable phases is a nonlinear, nonequilibrium problem, it is worth considering the extent to which nonlinearities and correlations in the microscopic dynamic are included in the proposed macroscopic dynamics. We, therefore, point out that although specifically *non*equilibrium correlations are not included by virtue of the loss of spatial resolution resulting from the projection of the dynamic onto the macroscopic order parameter, *equilibrium* correlations are included through their effect on the highly nonlinear restricted free energy $F(m)$. However, since in this paper we only consider a single macroscopic variable, effects of nonlinear interactions between macroscopic variables [29] are not included.

The rest of this paper is organized as follows. In Sec. II, we introduce our two specific macroscopic mean-field dynamics, emphasizing their common physical motivation. In Sec. III, we show how to obtain $F(m)$ using MC simulations. In Sec. IV, we summarize the relevant droplet-theory predictions for the decay of metastable phases. In Sec. V, we apply our macroscopic dynamics to the relaxation of the metastable phase in the two-dimensional ferromagnetic nearest-neighbor Ising model below its critical temperature. In Sec. VI, we discuss the connections between our results for the metastable lifetimes and the detailed shape of $F(m)$, with particular reference to earlier work [3,18-20]. Finally, in Sec. VII, we summarize our results and discuss some implications of this study.

## II. MACROSCOPIC MEAN-FIELD DYNAMICS

To set the stage for our study, we first consider the microscopic Metropolis dynamic for a mean-field Ising ferromagnet in which each spin interacts with equal strength with every other spin in the system. As was already shown by Griffiths *et al.* [22], this exactly defines a macroscopic dynamic that depends on the configurations of the system only through the restricted free energy $F(m)$. Next, for Ising models with finite interaction range, we propose two macroscopic dynamics, which can be constructed from $F(m)$ for the corresponding model while satisfying the two conditions introduced in Sec. I: (1) locality in $m$ and (2) correct static properties of $F(m)$. In proposing these dynamics we make as few specific physical assumptions as possible beyond the conditions (1)

and (2).

The ferromagnetic Ising model with equivalent-neighbor interactions is defined by the Hamiltonian

$$\mathcal{H} = -(J/N)\sum_{i<j} s_i s_j - H\sum_i s_i \,, \tag{2}$$

where $s_i=\pm 1$ are $N$ Ising spins, $H$ is an external magnetic field, and the sums $\sum_{i<j}$ and $\sum_i$ run over all $N$ spins with $1\le i<j\le N$ and $1\le i\le N$, respectively. For convenience we set the interaction constant $J$ equal to 1. The magnetization per spin,

$$m = N^{-1}\sum_i s_i \,, \tag{3}$$

is the order parameter conjugate to $H$, and the number of up spins is related to $m$ as

$$n = \frac{N}{2}(1+m) \,. \tag{4}$$

With these definitions, Eq. (2) can be written as [22]

$$\mathcal{H} = E(n) = -\frac{(2n-N)^2}{2N} - H(2n-N) + \tfrac{1}{2} \,. \tag{5}$$

We consider a microscopic Metropolis dynamic in which the spin at a randomly selected site $i$ is flipped from $s_i \to -s_i$ with probability

$$p(x \to x') = \exp\left(\min\{0, \beta[E(x) - E(x')]\}\right) , \tag{6}$$

where $E(x)$ and $E(x')$ are the energies of the microscopic spin configurations $x=\{s_j\}$ and $x'$ before and after the flip, respectively. The microscopic detailed-balance condition is satisfied [24]. For this model, the one-step transition probabilities $W_1(n,n')$ from states with order parameter $n$ to states with $n'$ are [22]

$$W_1(n,n+1) = \left(1-\frac{n}{N}\right)\exp\left(\min\{0,\beta[E(n)-E(n+1)]\}\right), \tag{7a}$$

$$W_1(n,n-1) = \frac{n}{N}\exp\left(\min\{0,\beta[E(n)-E(n-1)]\}\right), \tag{7b}$$

$$W_1(n,n) = 1 - W_1(n,n+1) - W_1(n,n-1) \,. \tag{7c}$$

Here the arguments of the matrix elements $W_1(n,n')$ are all between 0 and $N$, and matrix elements with arguments outside this range are identically zero. In this dynamic the probability for choosing an up (down) spin is $n/N$ $(1-n/N)$.

Since the value of $n$ in the equivalent-neighbor model uniquely specifies the energy of the spin configuration, $\beta E(n)$ can be replaced by $F(n)+S(n)$, where $F(n)$ is the restricted free energy [$F(n) \equiv \beta E(n) - S(n)$ with $\beta$ absorbed in $F$], and $S(n) = \ln\Omega(n)$ is the Boltzmann entropy for the density of states $\Omega(n) = N!/n!(N-n)!$. The probability that the system has $n$ up spins is proportional to $\exp[-F(n)]$ [31]. Equation (7) thus becomes

$$W_1(n,n+1) = \left(1-\frac{n}{N}\right)\exp\left(\min\{0,[F(n)-F(n+1) + S(n)-S(n+1)]\}\right), \tag{8a}$$

$$W_1(n,n-1) = \frac{n}{N}\exp\left(\min\{0,[F(n)-F(n-1) + S(n)-S(n-1)]\}\right), \tag{8b}$$

$$W_1(n,n) = 1 - W_1(n,n+1) - W_1(n,n-1) \,. \tag{8c}$$

Since $\exp[S(n)-S(n-1)] = (N-n+1)/n$, it is straightforward to show that

$$\frac{W_1(n,n')}{W_1(n',n)} = \exp[F(n)-F(n')] \,, \tag{9}$$

which can be considered to be the macroscopic detailed-balance condition between states with order parameter $n$ and $n'=n\pm 1$. Consequently, the equilibrium probability distribution for the order parameter $n$ resulting from this Metropolis dynamic is correctly proportional to $\exp[-F(n)]$.

Once the transition probability matrix $W_1(n,n')$, which for $N$ Ising spins is an $(N+1)\times(N+1)$ tridiagonal matrix, is constructed from $F(n)$, particular realizations of this stochastic process can be created, starting from an arbitrary initial state. The average first-passage time $\langle\tau\rangle$ to the globally stable phase, starting from a metastable phase, can be easily calculated from $W_1(n,n')$ by the methodology of absorbing Markov chains [32] (see Appendix B). Higher moments of the first-passage time $\tau$ can also be obtained by the same method. We again emphasize that for the equivalent-neighbor model, the time evolution of the macroscopic order-parameter distribution given by Eq. (8) is an *exact* consequence of the underlying microscopic dynamic [22].

Next, as a prototype ferromagnet with short-range interactions we investigate the nearest-neighbor square-lattice Ising model for which the Hamiltonian is

$$\mathcal{H} = -J\sum_{\langle i,j\rangle} s_i s_j - H\sum_i s_i \,, \tag{10}$$

where $s_i = \pm 1$ is the Ising spin at site $i$. The interaction constant $J$ will be set to one as before, periodic boundary conditions are used, and $H$ is the applied field [33]. The sums $\sum_{\langle i,j\rangle}$ and $\sum_i$ run over all nearest-neighbor pairs and over all $N=L^2$ sites on a square lattice. In contrast to infinite-range models, for models with *finite* interaction range, such as given by Eq. (10), Eq. (8) cannot be exactly derived from the microscopic Metropolis dynamic defined by Eq. (6), even if $F(n)$ is numerically calculated to give the correct functional form appropriate to the particular model. The reason for this is that the local environment with which a particular spin interacts is no longer uniquely determined by the macroscopic order parameter. Nevertheless, we can define a macroscopic dy-

namic for a particular short-range model through Eq. (8) with the appropriate form for $F(n)$ and consider it as an approximation for the true order-parameter dynamic observed in a microscopic MC simulation. This approximate macroscopic dynamic is our "mean-field dynamic No. 1" (MFD1). Although MFD1 is not exactly derived from any particular microscopic dynamic, it satisfies the two conditions of locality in the order parameter $m$ and correct static properties of $F(m)$, which we introduced in Sec. I.

We emphasize two important features of MFD1. First, regardless of the functional form of $F(m)$ for the particular microscopic model, this form is correctly reproduced by the dynamic. Second, MFD1 is not the only macroscopic dynamic capable of correctly yielding $F(m)$. This is analogous to the fact that there exist many different microscopic dynamics that can be successfully used to study the equilibrium properties of a single model. In fact, the macroscopic detailed-balance condition, Eq. (9), is sufficient to ensure that a dynamic yields $\exp[-F(m)]$ as its equilibrium distribution. Perhaps the simplest Metropolis-type dynamic that satisfies both Eq. (9) and our requirement of locality in $m$ is defined by the transition-matrix elements,

$$W_2(n,n+1) = \tfrac{1}{2}\exp[\min\{0, F(n) - F(n+1)\}], \quad (11a)$$

$$W_2(n,n-1) = \tfrac{1}{2}\exp[\min\{0, F(n) - F(n-1)\}], \quad (11b)$$

$$W_2(n,n) = 1 - W_2(n,n+1) - W_2(n,n-1) , \quad (11c)$$

where the range of the arguments is the same as for $W_1$, and $W_2$=0 for out-of-range arguments. These transition probabilities define our "mean-field dynamic No. 2" (MFD2).

In Sec. V, we compare the macroscopic order-parameter dynamic observed in MC simulations of the two-dimensional Ising ferromagnet with the microscopic Metropolis dynamic defined by Eq. (6) to our approximate macroscopic dynamics, MFD1 and MFD2. This allows us to investigate the relevance of the equilibrium properties of a system to the dynamical relaxation behavior of its metastable phases.

## III. RESTRICTED FREE ENERGY BY MONTE CARLO SIMULATIONS

In this section, we describe how to obtain, from microscopic, equilibrium MC simulations, the bulk restricted free energy $F(m)$, which is defined through the restricted partition function

$$\exp[-F(m)] = \sum_x \delta(m(x) - m)\exp[-\beta E(x)] , \quad (12)$$

where the sum is over all possible *microscopic* spin configurations $x$, and $\delta$ is the Kronecker $\delta$ function. It is straightforward to show that the probability distribution for $m$ is proportional to $\exp[-F(m)]$ [31]. For Ising models with short-range interactions below the critical temperature $T_c$, $F_0(m)$ [i.e., $F(m)$ for $H$=0, as defined in Eq. (1)] has two symmetrical minima, and the bulk free-energy barrier separating these minima diverges as the linear system size $L$ for $L \gg 1$ in two dimensions (as $L^{d-1}$ in $d$ dimensions) [3,31].

Recently, significant progress has been achieved in the search for more efficient MC sampling algorithms for systems in which different subsets of phase space are separated by large free-energy barriers [3,34–41]. Here we use a variation of the multicanonical method [38–40], employing the notation of Ref. [41].

The partition function for $H$=0 and inverse temperature $\beta$ is

$$Z(\beta, H=0) = \sum_{E,M} \exp[S(E,M) - \beta E] = \sum_M \exp[-F_0(M)] , \quad (13)$$

where

$$\exp[-F_0(M)] \equiv \sum_E \exp[S(E,M) - \beta E] , \quad (14)$$

$\exp[S(E,M)]=\Omega(E,M)$ is the density of states, and $E$ and $M=mL^2$ are the bulk internal energy and magnetization, respectively.

The detailed-balance condition for the MC simulation can be written as

$$\frac{W(x \to x')}{W(x' \to x)} = \exp\left[-\beta\{E(x') - E(x)\} - \left\{\tilde{J}(M(x')) - \tilde{J}(M(x))\right\}\right] , \quad (15)$$

where $\tilde{J}$ can be any arbitrary function of $M$. For an ergodic MC algorithm, the resulting distribution (histogram) of the sampling has been shown [41] to be

$$\tilde{H}(E,M) \propto \exp[S(E,M) - \beta E - \tilde{J}(M)] . \quad (16)$$

From Eqs. (14) and (16) we get

$$\tilde{H}(M) = \sum_E \tilde{H}(E,M) \propto \exp[F_0(M) - \tilde{J}(M)] . \quad (17)$$

Therefore,

$$F_0(M) = \tilde{J}(M) + \ln \tilde{H}(M) \quad (18)$$

up to an additive constant.

As in Ref. [41], the quantity $F_0(M)$ can be obtained using Eq. (18) in an iterative fashion. The old estimates of $F_0(M)$ and $\tilde{J}(M)$ can be used in a MC procedure to obtain a new histogram and, consequently, a new and better estimate for $F_0(M)$ from Eq. (18). Although this approach is more efficient than conventional sampling methods [40], we find that it does not suffice to obtain $F_0(M)$ at very low temperatures. This is due to the large size of the exponent in Eq. (15) for large $\beta$.

As in Ref. [41], we instead sample the Boltzmann entropy $S(E,M)$ directly by imposing the detailed-balance condition

$$\frac{W(x \to x')}{W(x' \to x)} = \exp\left[\hat{J}(E(x),M(x)) - \hat{J}(E(x'),M(x'))\right] , \tag{19}$$

which yields the histogram

$$\tilde{H}(E,M) \propto \exp[S(E,M) - \hat{J}(E,M)] . \tag{20}$$

Therefore, $S(E,M)$ can be obtained, up to an additive constant, by iteratively evaluating

$$S(E,M) = \hat{J}(E,M) + \ln \hat{H}(E,M) \tag{21}$$

where $\hat{J}(E,M)$ is an input and $\hat{H}(E,M)$ is the resulting histogram of $\hat{J}(E,M)$ from Eq. (19). Once $S(E,M)$ has been obtained to the desired accuracy, $F_0(M)$ can be obtained from Eq. (14) for any $\beta$. We were able to obtain $F_0(M)$ for any $\beta > \beta_c$ for the nearest-neighbor Ising ferromagnet on $L \times L$ square lattices with $L \leq 24$. The $H$-dependent $F(m)$ are trivially constructed from $F_0(m)$ by Eq. (1).

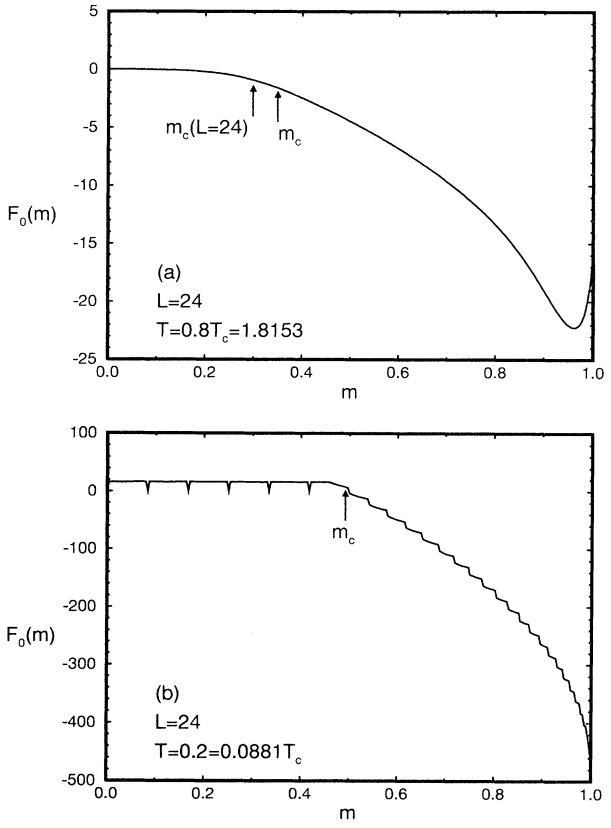


FIG. 1. (a) The zero-field bulk restricted free energy, $F_0(m)$, of the nearest-neighbor Ising ferromagnet on a square lattice at $T=0.8T_c=1.8153\ldots$ for $L=24$. (b) Same as (a), but at $T=0.2 \approx 0.0881T_c$. Notice the difference in the scales along the $y$ axis in (a) and (b). The sawtoothlike behavior of $F_0(m)$ at $T=0.2$ is due to the discreteness of the lattice. The vertical arrows marked $m_c$ indicate the exactly known magnetization for which the most likely configuration with the given magnetization changes from a slab (for $|m| < m_c$) to a droplet (for $|m| > m_c$) in an infinite system [42].

In Fig. 1 we show $F_0(m)$ for $T=0.8T_c \approx 1.8153$ [Fig. 1(a)] and for $T=0.2 \approx 0.0881T_c$ [Fig. 1(b)]. The sawtoothlike behavior of $F_0(m)$ for $T=0.2$ is due to the discreteness of the lattice. For $T=0.8T_c$, we used Eq. (15) to obtain $F_0(m)$ for lattices up to $L=64$. The vertical arrows marked $m_c$ indicate the exactly known magnetization for which the most likely configuration with the given magnetization changes from a slab (for $|m| < m_c$) to a droplet (for $|m| > m_c$) in an infinite system [42]. In Fig. 1(a), we have also marked the value of $m_c$ corresponding to $L=24$, taken from Fig. 3 of Ref. [42]. For further discussion of the droplet-to-slab transition and its significance, see Sec. VI.

## IV. DROPLET THEORY AND ITS PREDICTIONS

In this section, we review some predictions of droplet theory for the metastable lifetime $\langle \tau \rangle$ in $d$-dimensional ferromagnetic systems with short-range interactions and local dynamics [33]. We leave details of the theory to Refs. [1,5] and the references cited there. Starting with a large magnetization opposite to the applied field, we consider its relaxation and define $\langle \tau \rangle$ as the average time it takes for $m(t)$ to reach a particular cutoff value, $m_{\rm cut}$.

In addition to the lattice constant, which we take as unity, five length scales are important in the droplet theory for relaxation of metastable phases. These are the linear system size $L$, the radius of the critical droplet $R_c$, the average distance between supercritical droplets $R_0$, and the single-phase correlation lengths in the stable and metastable phases, $\xi_{\rm s}$ and $\xi_{\rm ms}$, respectively. Since the temperatures of interest in the present study are well below $T_c$, $\xi_{\rm s}$ is practically field independent and of the order of unity, and since the field strengths considered are moderate, the same is the case for $\xi_{\rm ms}$ [12]. Thus we are left to consider the interplay between three lengths: $L$, $R_0$, and $R_c$, all of which are larger than unity in the temperature and field regimes of interest.

By comparing the bulk free energy gained by creating a droplet of the equilibrium phase in the metastable background with the free-energy cost of creating the droplet surface, one can show that the critical radius, beyond which the droplet is more likely to grow than to shrink, is

$$R_c = \frac{(d-1)\sigma_0(T)}{\Delta m |H|} \approx \frac{(d-1)\sigma_0(T)}{2m_{\rm eq}(T)|H|} , \tag{22}$$

where $\Delta m$ is the magnetization difference between the metastable and the stable phase, and $m_{\rm eq}(T)$ is the spontaneous equilibrium magnetization. Also, $\sigma_0(T)$ is the equilibrium surface tension along a primitive lattice vector, and is assumed to be equal to the surface tension in the metastable phase. For the two-dimensional Ising model, both $\sigma_0(T)$ [43] and $m_{\rm eq}(T)$ [44] are exactly

known. The relaxation proceeds in different ways, depending on the relative sizes of $L$, $R_0$, and $R_c$.

If $|H|$ is sufficiently small that $R_c > L$, then the saddle-point configuration is a slab spanning the system in $d-1$ dimensions, and $L$ is the most important length scale for the relaxation. The metastable lifetime is then determined by the surface free energy of such a slab. Consequently, for periodic boundary conditions it increases with $L$ as [45–47]

$$\langle \tau(T,H,L) \rangle \sim \exp\left[2\beta\sigma_0(T)L^{d-1}\right] . \tag{23}$$

This region of ultraweak fields is called the "coexistence" (CE) region [5], since the dynamic is similar to that at $H=0$, where two competing bulk phases coexist.

As $|H|$ is increased, $R_c$ becomes smaller than $L$. The crossover to the field regimes where the relaxation is dominated by critical droplets smaller than $L$ has been called the "thermodynamic spinodal" (THSP) [4]. The crossover field $H_{\rm THSP}$ can be estimated by requiring that the critical droplet should occupy a volume fraction

$$\phi = \left(1 - \frac{m}{m_{\rm eq}(T)}\right) \tag{24}$$

corresponding to the cutoff magnetization $m_{\rm cut}$. This yields [1,5]

$$H_{\rm THSP}(\phi) = \frac{1}{L}\left[\frac{(d-1)\Xi(T)}{2m_{\rm eq}(T)\phi}\right]^{1/d} , \tag{25}$$

where $\Xi(T)$ can be calculated from $m_{\rm eq}$ and the anisotropic equilibrium surface tension by the equilibrium Wulff construction [43,48] to obtain the critical droplet shape [11,12,49].

For fields somewhat stronger than $H_{\rm THSP}$, so that $L \gg R_c \gg 1$, the nucleation rate per unit volume for critical droplets becomes [8–10,17]

$$\Gamma(T,H) \propto |H|^{b+c} \exp\left[\frac{-\beta\Xi(T)}{|H|^{d-1}}\left\{1+O(H^2)\right\}\right] . \tag{26}$$

The exponent $b$ is a universal exponent related to excitations on the droplet surface, and the nonuniversal exponent $c$ gives the $H$ dependence of a "kinetic prefactor" [8–10] which contains all dependence on the details of the dynamics. For $d=2$ and 3, it is expected that $b=1$ and $-7/3$, respectively [17]. This has been confirmed by several methods, most recently by constrained-transfer-matrix calculations [11,12]. For dynamics that can be described by a Fokker-Planck equation, it is expected that $c=2$ [9,10,17]. In a recent MC study for $d=2$, it was confirmed that $b+c \approx 3$ for the Metropolis dynamic with updates at randomly chosen sites [5].

If $R_0 \gg L \gg R_c$, a single critical droplet is sufficient for macroscopic decay to occur before additional droplets nucleate. This region is called the "single-droplet" (SD) region [5]. Assuming that the exact value of $m_{\rm cut}$ is not an important factor (see the discussion in Ref. [5]), the average relaxation time $\langle \tau \rangle$ to $m_{\rm cut}$ can be written as

$$\begin{aligned}\langle \tau(T,H,L) \rangle &\approx \left[L^d \Gamma(T,H)\right]^{-1} \\ &\propto L^{-d}|H|^{-(b+c)} \\ &\quad \times \exp\left[\frac{\beta\Xi(T)}{|H|^{d-1}}\left\{1+O(H^2)\right\}\right] .\end{aligned} \tag{27}$$

This leads to

$$\Lambda(T,H) \equiv \frac{d\ln\langle \tau(T,H,L)\rangle}{d|H|^{1-d}} = \beta\Xi(T) + \frac{b+c}{d-1}|H|^{d-1} , \tag{28}$$

where we have neglected higher-order correction terms.

If $L \gg R_0 \gg R_c$, many critical droplets nucleate before the decay of the order parameter can proceed to a macroscopic extent. This region is called the "multidroplet" (MD) region [5]. In this region, we expect $\langle \tau \rangle$ to be independent of $L$. With the assumption that the radial growth velocity of the supercritical droplets is proportional to the applied field $H$ [50–52], $\langle \tau \rangle$ is predicted to be [5,53–57]

$$\begin{aligned}\langle \tau(T,H) \rangle &\sim |H|^{-\frac{b+c+d}{d+1}} \\ &\quad \times \exp\left[\frac{\beta\Xi(T)}{(d+1)|H|^{d-1}}\left\{1+O(H^2)\right\}\right] ,\end{aligned} \tag{29}$$

which leads to

$$\Lambda(T,H) = \frac{\beta\Xi(T)}{d+1} + \frac{b+c+d}{d^2-1}|H|^{d-1} , \tag{30}$$

where higher-order corrections again have been neglected. One also has the mean droplet distance [5,56,57]

$$\begin{aligned}R_0(T,H) &\propto |H|^{-\frac{b+c-1}{d+1}} \\ &\quad \times \exp\left[\frac{\beta\Xi(T)}{(d+1)|H|^{d-1}}\left\{1+O(H^2)\right\}\right] .\end{aligned} \tag{31}$$

The field $H_{\rm DSP}$, which separates the SD and MD regions was called the "dynamic spinodal field" in Refs. [4,5]. It can be estimated by setting $R_0(T,H) \propto L$ with a proportionality constant of order unity, which gives the scaling relation,

$$\begin{aligned}H_{\rm DSP} = \left(\frac{\beta\Xi(T)}{(d+1)\ln L}\right)^{\frac{1}{d-1}} &\left[1 + O\left(\frac{\ln(\ln L)}{\ln L}\right)\right. \\ &\left. + O\left(\frac{1}{\ln L}\right)\right] ,\end{aligned} \tag{32}$$

expected to be asymptotically valid for nonzero $T$.

These droplet-theoretical results can be summarized as follows. For a given system size $L$, if $|H|$ is small enough so that $R_c > L$, then $L$ is the most important length scale for the relaxation, and the system is in the CE region. As $|H|$ is increased beyond $H_{\rm THSP}$, $R_c$ becomes smaller than $L$. If $R_0 \gg L \gg R_c$, the system is in the SD region, and the relaxation is characterized by Eq. (28), from which one can estimate $b+c$ and $\Xi(T)$. As $|H|$ is increased still further, so that $R_c \ll R_0 \ll L$, the system is in the MD re-

gion. The relaxation is then characterized by Eq. (30), from which one again can estimate $b+c$ and $\Xi(T)$. The crossover field that separates the SD and MD regions, $H_{\rm DSP}$, also separates the "stochastic region" and the "deterministic region" [4]. In the "deterministic" region, the average metastable lifetime $\langle\tau\rangle$ is quite short, and the standard deviation of $\tau$ is much smaller than $\langle\tau\rangle$. In the "stochastic" region, the decay approximately follows a Poisson process, so that the standard deviation of $\tau$ is comparable to $\langle\tau\rangle$. As $|H|$ becomes very large, the droplet picture becomes inappropriate, and $R_0$ and $R_c$ become comparable to the lattice spacing. The lifetime is then on the order of one MC step per site (MCSS), and this region is called the "strong-field" (SF) region. The crossover between the MD and SF regions is marked by the "mean-field spinodal field" $H_{\rm MFSP}$ [4], which can be estimated as the field at which $2R_c=1$ [12]. In Fig. 2, we show a schematic diagram for the relaxation behavior, illustrating the four subregions of characteristic relaxation behavior predicted by droplet theory.

For low temperatures, the discreteness of the lattice becomes important. It has been shown [58–63] that for sufficiently low temperatures, the lifetime of the metastable

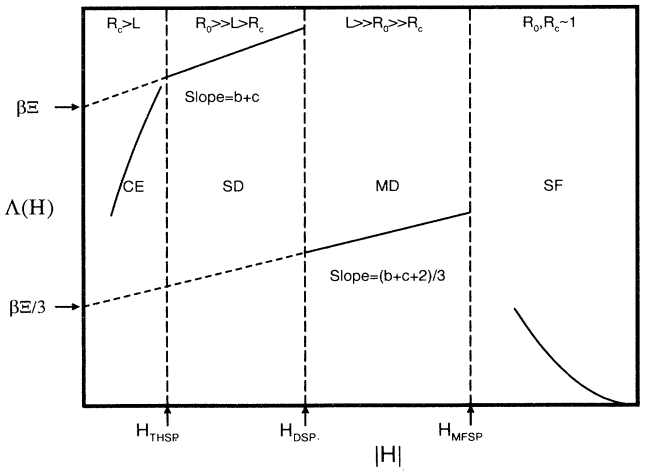


FIG. 2. Schematic plot of $\Lambda(H)$, defined in Eq. (28), for a two-dimensional Ising ferromagnet. The dynamic spinodal field $H_{\rm DSP}$ separates the stochastic and the deterministic regions. In the stochastic region ($|H|<H_{\rm DSP}$), the relaxation time $\langle\tau\rangle$ is determined by the formation of a single critical droplet. Depending on the size of the critical droplet relative to the system size, the stochastic region is divided into the single-droplet (SD) and coexistence (CE) subregions. In the SD region the size of the critical droplet is smaller than the system size. The CE region is also characterized by a single nucleating droplet, but of a size comparable to the system size. The thermodynamic spinodal field $H_{\rm THSP}$ separates the SD and CE regions. The deterministic region ($|H|>H_{\rm DSP}$) is comprised of the multidroplet (MD) and strong-field (SF) regions. These two regions are separated by the mean-field spinodal (MFSP). Droplet theory [5] predicts that the intercepts of the two straight lines are $\beta\Xi$ and $\beta\Xi/3$. Their slopes are related as shown in the figure if one assumes that the radial growth velocity of the supercritical droplets is proportional to $H$.

phase for the nearest-neighbor square-lattice Ising ferromagnet with Hamiltonian given by Eq. (10) is given by

$$\ln\langle L^2\tau\rangle = 8\beta l_c - 2\beta|H|(l_c^2 - l_c + 1)\ , \tag{33}$$

where the size of the critical droplet is $l_c = \lceil 2/|H|\rceil$ and the notation $\lceil x\rceil$ denotes the smallest integer greater than $x$. This result is restricted to $2/|H|$ not being an integer and to $|H|<4$. For this result to be valid the temperature must be at least low enough and the lattice size large enough to insure that the system is in the SD region. Differentiating Eq. (33) with respect to $|H|^{-1}$ gives

$$T\Lambda = 2H^2(l_c^2 - l_c + 1)\ . \tag{34}$$

## V. NUMERICAL RESULTS

In this section, we present extensive results of the mean-field dynamics introduced in Sec. II for the relaxation behavior of the metastable phase in the nearest-neighbor Ising ferromagnet on a square lattice with the Hamiltonian given in Eq. (10). Periodic boundary conditions are used throughout.

First, we consider $T=0.8T_c$ ($\beta=0.55086\ldots$) for direct comparison with recent MC results [5]. We obtained $F_0(m)$ for the entire range of $-1 \le m \le +1$ for system sizes up to $64\times64$, using the method outlined in Sec. IV and utilizing the Ising spin-reversal symmetry $F_0(m) = F_0(-m)$. For $H \neq 0$, $F(m)$ was obtained from Eq. (1). Once $F(m)$ was obtained, the Markov transition probability matrices $\mathbf{W}_1$ and $\mathbf{W}_2$ for the two dynamics MFD1 and MFD2 were constructed through the procedure outlined in Sec. II. We show the results from MFD1 first and discuss MFD2 later. As in Ref. [5], the initial state is chosen as $m=+1$ with $H<0$, and an absorbing barrier is put at $m_{\rm cut}=0$. In Ref. [5], different values of $m_{\rm cut}$ were also used. As long as $m_{\rm cut}$ is sufficiently far away from the metastable value of $m$ that the largest droplet must already be supercritical, the precise value of $m_{\rm cut}$ is not important for weak fields [5].

Using the absorbing Markov chain method discussed in Appendix B, the average first-passage time $\langle\tau\rangle$ to $m=m_{\rm cut}$ and the standard deviation $\sigma_\tau \equiv \sqrt{\langle\tau^2\rangle - \langle\tau\rangle^2}$ were obtained by matrix inversion using the computer subroutine TRIDAG from Ref. [64]. Our values of $\tau$ were divided by $L^2$ to give all times in units of MCSS.

In Fig. 3, we show the relaxation time, defined as the first-passage time to $m_{\rm cut}=0$, obtained from MFD1 for $L=32$ and 64. For comparison, MC results for the standard Metropolis algorithm with spin updates at randomly chosen sites for $L=32$ and 64 are also plotted. We find that MFD1 and the microscopic MC simulations give qualitatively similar results for the relaxation time.

In Fig. 4, we show the slope $\Lambda$ of the data in Fig. 3 with respect to $|H|^{-1}$, whose asymptotic values in the SD and MD regions are given in Eqs. (28) and (30), respectively. We clearly see four distinct relaxation regions for $L=64$. The SF region, $|H|>H_{\rm MFSP}$ ($H_{\rm MFSP}(0.8T_c)\approx0.75$ [12]), contains the sharp peak for very small $|H|^{-1}$ in Fig. 4(b).

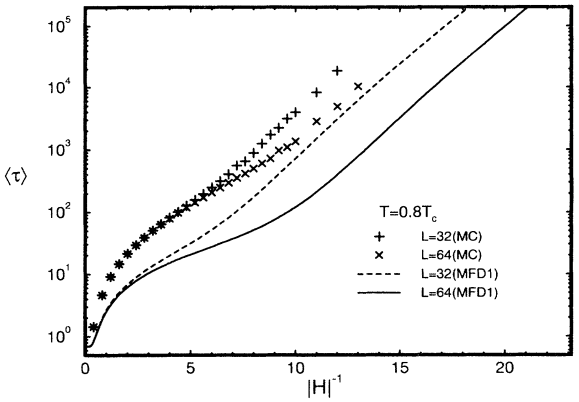


FIG. 3. The field dependence of the average metastable lifetime $\langle\tau\rangle$ for a two-dimensional Ising model at $T=0.8T_c$. The lifetime $\langle\tau\rangle$ is estimated as the average first-passage time to $m_{\rm cut}=0$ from the starting configuration $m=+1$ with $H<0$. The lines correspond to the MFD1 dynamic for $L=32$ (dashed) and 64 (solid). The results of Metropolis MC simulations with random site updates for $L=32$ and 64 are marked by + and ×, with $10^3$ escapes from the $m=+1$ state. The statistical errors are smaller than the symbol size.

[Figure 4(a) is analogous with the schematic Fig. 2, in which the various field regions and crossover fields are indicated.] The region $0.2\lesssim|H|\lesssim0.75$ corresponds to the MD region. As $|H|$ is lowered, the crossover from the MD region to the SD region is signaled by a sudden rise in $\Lambda$. In Fig. 4(a), we define $H_{\rm max}$ and $H_{\rm min}$ as the fields at which $\Lambda$ has a local maximum and minimum, respectively. As $|H|$ is lowered further, $\Lambda$ plunges towards zero, signaling the CE region. From our numerical data for MFD1 we find this crossover field $H_{\rm THSP}$ at about $|H|^{-1}\approx40$ for $L=64$ and $|H|^{-1}\approx20$ for $L=32$. [See Fig. 4(b).] This is consistent with the relation $H_{\rm THSP}\propto L^{-1}$ given in Sec. III. For further discussion of the thermodynamic spinodal and its relation to the droplet-to-slab transition, see Sec. VI.

Using the numerically exact value [43,48] of $\Xi$, we find our results consistent with $b+c\approx2$ for MFD1, based on the data in the SD region. The expected value for dynamics that can be described by a Fokker-Planck equation is $b+c=3$. The estimate $b+c\approx2$ for MFD1 at $0.8T_c$ should be taken with extreme caution, since the asymptotic region for $L=64$ appears to be quite small. For a more reliable estimate, we would need results from larger systems at this temperature. Since we have difficulties in obtaining $F(m)$ for larger system sizes, we instead tested Eq. (28) at lower temperatures, assuming that $b+c$ does not depend on the temperature. Although the accessible system sizes are smaller for lower temperatures, due to the difficulties in estimating $S(E,M)$ for all values of $E$ and $M$, this approach turns out to be a more reliable way with our dynamics to estimate $b+c$. These studies at lower $T$ are also consistent with $b+c\approx2$, as discussed below.

Although the results from the mean-field dynamic are in good overall agreement with those from the MC simulations, the quantitative estimates of the intercept and the slope in Fig. 4(a) are less satisfactory for the MD region. Since the asymptotic region, in which Eq. (30) is valid for MC simulations at $0.8T_c$, has been shown to be relatively narrow, even for $L=720$ [5], results for much larger system sizes than $L=64$ would be necessary to provide a satisfactory test of Eq. (30) for the mean-field dynamics at this temperature. At lower temperatures we are nevertheless able to estimate below that $b+c\approx2$ for MFD1 in the SD region, and this gives the slopes drawn in Fig. 4(a) for both regions. In contrast, it was demonstrated in Ref. [5] for systems with $L\leq720$ that Metropolis MC simulations with spin updates at randomly selected sites give $b+c\approx3$, in agreement with theoretical expectations [9,10,17]. The apparent consistency with $b+c\approx2$ of the Metropolis MC results for $L=64$, which are also shown in Fig. 4(a), is, therefore, clearly

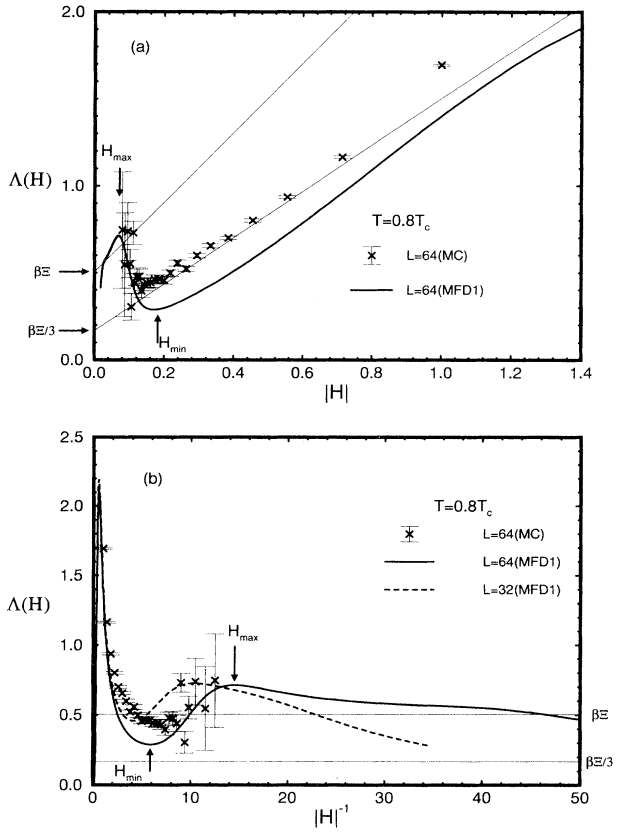


FIG. 4. (a) The slope $\Lambda(H)$, obtained from the data in Fig. 3, shown as a function of $|H|$. The thick solid curve is from MFD1 for $L=64$, and the symbols are from the standard Metropolis MC simulations with random site updates for $L=64$. The two straight lines are drawn with slopes $b+c=2$ and $(b+c+2)/3=4/3$, using the exact value [43,48] of $\beta\Xi(0.8T_c)=0.5062\ldots$. The horizontal arrows mark the exact values of $\beta\Xi(0.8T_c)$ and $\beta\Xi(0.8T_c)/3$. The asymptotic SD subregion seems to be very small for $L=64$. The SF subregion ($|H|>2$), where $\Lambda(H)$ decreases to zero is not shown. We define $H_{\rm max}$ and $H_{\rm min}$ as the fields at which $\Lambda$ has a local maximum and minimum, respectively. (b) The slope $\Lambda(H)$, shown as a function of $|H|^{-1}$. The two horizontal lines correspond to the exact values of $\beta\Xi$ and $\beta\Xi/3$. The interpretations of the other lines and symbols are the same as in (a).

due to finite-size effects.

In Fig. 5, we show the field dependence of the slope $\Lambda$ obtained from MFD1 and MFD2 at $T=0.8T_c$. Both are in qualitative agreement with Fig. 2. The SF region, where $\Lambda$ decreases to zero for large $|H|$, is not shown. Figure 5 provides some insight about the relevance of $F(m)$ and the possible artificial results from the mean-field dynamics. The fact that Fig. 5 is in qualitative agreement with Fig. 2 indicates the importance of $F(m)$ for the dynamics. However, as one might expect from the sensitive dependence of the kinetic-prefactor exponent $c$ on the details of the dynamic, which was demonstrated in Ref. [5], values of $b+c$ obtained from mean-field dynamics do not correctly reflect that of the underlying microscopic dynamic. In the SD region, $\Lambda$ approaches the exact value $\beta\Xi$ with a slope that depends on the details of the particular dynamic. For MFD1 and MFD2, $b+c$ is about 2.0 and 3.7, respectively. In the MD region for both MFD1 and MFD2, we find only qualitative agreement with droplet-theory predictions. As will be explained in Sec. VI, it is expected that only in the SD region can quantities related to the metastable phase be reliably extracted from $F(m)$. In the MD region, $\Lambda$ depends strongly on the details of the particular dynamic, and the dynamics associated with the droplet growth is not taken into account correctly in $F(m)$. Note that the MD region is fairly easily accessible by standard MC simulations, since $\tau$ there is rather small.

In Fig. 6, we show the field dependence of the relative standard deviation of the lifetime,

$$r = \sigma_\tau/\langle\tau\rangle\ , \tag{35}$$

which provides additional information about how the metastable phase decays. If the decay of the metastability involves a single Poisson process of forming one critical droplet, as is the case in the SD region, we expect $r\approx 1$. In the MD region, on the other hand, one needs to consider many independent Poisson processes. By partitioning the system into $(L/R_0)^2 \gg 1$ cells of volume proportional to $R_0^2$, one gets $r \propto R_0/L$, where $R_0$ is given by Eq. (31) [5,65]. A more rigorous argument, based on the two-point correlation function [57], can be found in the appendix of Ref. [65]. An estimate for the crossover field $H_{\rm DSP}$ between the SD and MD regions can be chosen as the field $H_{1/2}$, for which $r=1/2$ [4,5]. For further discussion of the dynamic spinodal in mean-field dynamics, see Sec. VI.

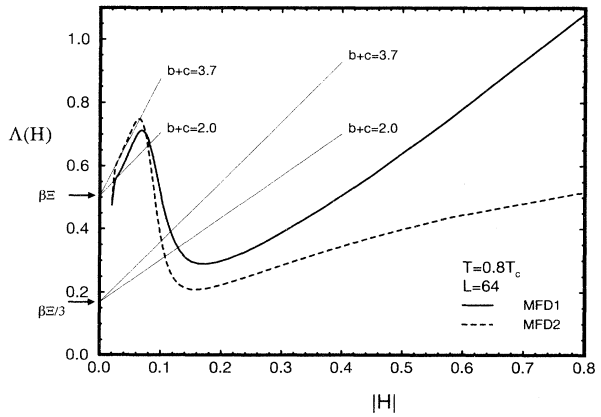


FIG. 5. The field dependence at $T=0.8T_c$ of $\Lambda(H)$ for the two different mean-field dynamics, MFD1 and MFD2. Qualitatively similar behavior is observed for both dynamics. Using the exact value of $\beta\Xi$, we estimate in the SD region $b+c\approx 2.0$ and 3.7 for MFD1 and MFD2, respectively. In the MD region, the lifetimes for MFD2 are shorter than for MFD1. Even though the system size is too small to discuss the asymptotic behavior in the MD region, the results from MFD1 and MFD2 are not in good agreement with droplet theory in this region.

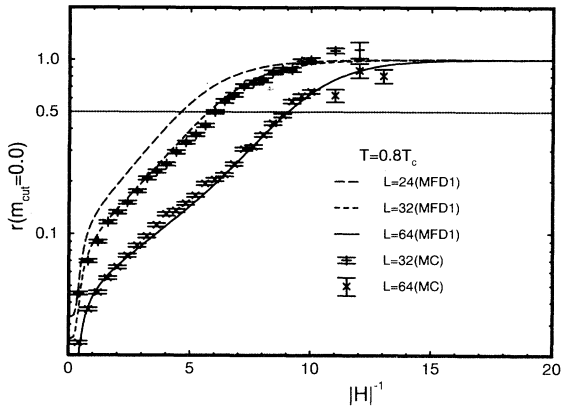


FIG. 6. The field dependence of the relative standard deviation $r=\sigma_\tau/\langle\tau\rangle$ at $T=0.8T_c$. The curves are from MFD1 for $L=24$, 32, and 64. The symbols are from the Metropolis MC simulations with random site updates for $L=32$ and 64. The MC data are from 3000 escapes from the metastable state near $r\approx 1/2$, and at least 100 escapes from the metastable state for the other $H$ values.

In Fig. 7(a), we show the temperature dependence of $H_{1/2}$ for $L=24$. The MC values lie between the estimates from MFD1 and MFD2. Again we considered the standard Metropolis dynamic with spin updates at randomly chosen sites. The MC simulations in this case were accelerated by using the method of absorbing Markov chains. This new MC method [6] generalizes the $n$-fold way algorithm [66,67] and gives large CPU-time savings for low temperatures without changing the underlying dynamics.

Analytic estimates for $H_{\rm DSP}$ at low temperatures can be obtained as follows. For sufficiently low temperatures, there exists a field $2<|H|<4$ such that a single overturned spin is a supercritical droplet [58–63]. We define $\tau_1$ as the average time before a single overturned spin appears. Further, we define $\tau_2$ as the average first-passage time from the state with a single overturned spin to the absorbing state with magnetization $m_{\rm cut}=0$. For $2<|H|<4$ and low temperatures, the processes that determine $\tau_2$ are deterministic, and for both MFD1 and MFD2, $\tau_2$ is of order unity. Using the free-energy difference between the state with a single overturned spin and the metastable state with no overturned spins, $2\beta|H| - 8\beta + \ln N$, one can obtain $\tau_1$ for MFD1 and MFD2 from Eqs. (8) and (11), respectively. We get $\tau_1 \propto \exp(8\beta - 2\beta|H| - \ln N)$ for MFD1 and $\tau_1 \propto \exp(8\beta - 2\beta|H| - 2\ln N)$ for MFD2. Note that we here give $\tau_1$ in units of MCSS and that $N=L^2$. The waiting time $\tau_1$ can be either large com-

pared to $\tau_2$, corresponding to stochastic decay, or small, corresponding to deterministic decay. Therefore, the estimate for $H_{\rm DSP}$ can be obtained by setting $\tau_1$ to be of the same order of magnitude as $\tau_2$, which leads to

$$4 - H_{\rm DSP} = \begin{cases} T(\ln L + c_1) & \text{for MFD1} \quad (36a) \\ T(2\ln L + c_2) & \text{for MFD2}\ , \quad (36b) \end{cases}$$

where $c_1$ and $c_2$ are nonuniversal constants. For MC simulations, $\tau_1 \propto \exp(8\beta - 2\beta|H| - \ln N)$ as for MFD1. Simulations in which the update sites are chosen sequentially give $\tau_2$ on the order of unity, so that $H_{\rm DSP}$ is given by Eq. (36a) for these microscopic dynamics as well. When updates are performed at randomly chosen sites, however, $\tau_2$ increases with $L$. The radial growth velocity $v$ is independent of $L$ and $H$ for $2<|H|< 4$ and $T \ll 1$, so that $v\tau_2 = O(L)$, and $\tau_1 = \tau_2$ then gives

$$4 - H_{\rm DSP} = T(\tfrac{3}{2}\ln L + c_3)\ . \quad (36c)$$

In Fig. 7, we compare these analytic low-temperature estimates for $H_{\rm DSP}$ with $H_{1/2}$ as obtained both from our mean-field dynamics and from microscopic MC simulations. Excellent agreement for the linear $T$ dependence is demonstrated in Fig. 7(a) and for the logarithmic $L$ dependence in Fig. 7(b).

In Fig. 8, we show the field dependence of the slope $\Lambda$ for $L$=24 as a function of $|H|$ for $T$=1.0, 1.1, and 1.2 in the SD region. (Note that $T_c$=2.269. . . .) We observe that, as expected, the size of the asymptotic SD region increases significantly as $T$ is lowered. The size of the MD subregion, which is not shown, is very compressed for these low temperatures, since the entropic factor is much less important in $F(m)$. From Fig. 8 we confirm that $b$+$c$=2.0(1) for MFD1 and $b$+$c$=3.7(2) for MFD2. To obtain these estimates of $b$+$c$ and $\beta\Xi$, we performed least-squares fits to Eq. (30) considering only data points in the asymptotic SD region in the following way. We first discarded data in the CE region. We then estimated the slopes and the intercepts as we successively removed data points from the strong-field end of the $|H|$ interval. Since the asymptotic region for Eq. (30) corresponds to $H_{\rm THSP}<|H|\ll 1$, our estimates for the slopes and the intercepts approached constant values with small fluctuations as we removed data points. Due to the uncertainty in $S(E,M)$, it is not easy to obtain a systematic error analysis. We, therefore, estimated the errors from the fluctuations of the estimates in the asymptotic region. The resulting estimates for $\beta\Xi$ from MFD1 are slightly different from those of MFD2, as shown in Fig. 8. The final error bars in our estimates for $\beta\Xi$ include this effect. Our estimates for $\beta\Xi$, 4.95(2), 4.00(1), and 3.20(2) for $T$=1.0, 1.1, and 1.2, respectively, are within 1% of the

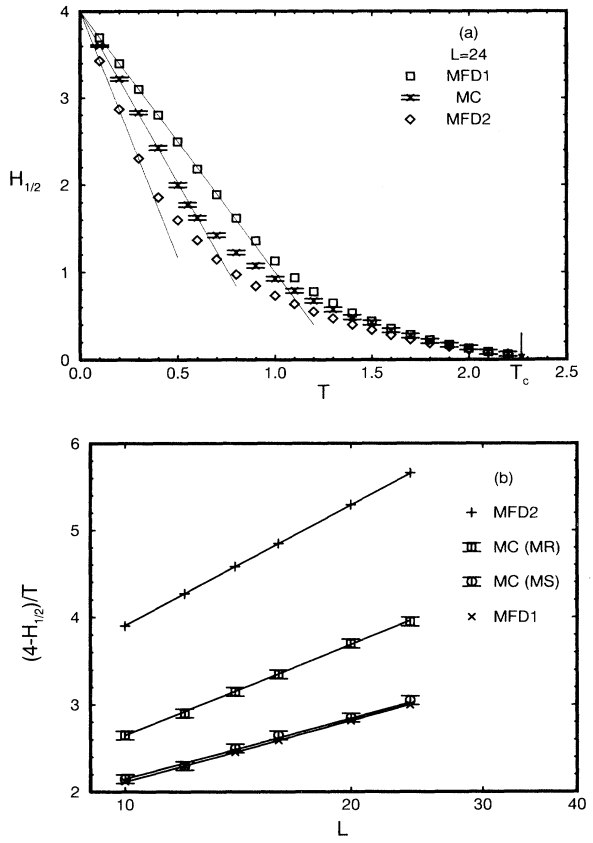


FIG. 7. (a) The temperature dependence of the estimate for the dynamical spinodal field $H_{\rm DSP}$, given by $H_{1/2}$ for $L$=24. Note that the MC simulation results (Metropolis with updates at randomly selected sites, MR) fall between the MFD1 and MFD2 results. The estimates approach $H$=4 linearly in $T$ with negative slopes, which depend on the system size $L$ and a nonuniversal constant. The slopes of the straight lines are 5.7, 4.0, and 3.0. (b) The asymptotic slopes near the point $(T, H_{1/2})$=(0, 4) as functions of $L$. We also show the MC results from the microscopic Metropolis algorithms with sequential (MS) and random (MR) spin updates. For comparison we show straight lines with the predicted slopes (2, 1.5, and 1 from top to bottom), obtained from the analytic low-temperature estimates for $H_{\rm DSP}$ in Eq. (36).

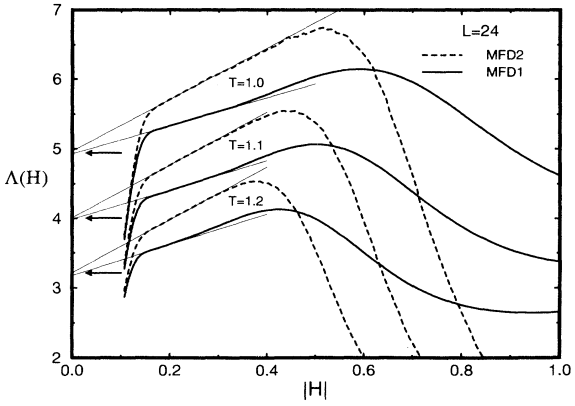


FIG. 8. The field dependence of the slope $\Lambda(H)$ for $L$=24 and $T$=1.0, 1.1, and 1.2. The size of the asymptotic SD region increases as $T$ is lowered. We estimate $b$+$c$ = 2.0(1) and 3.7(2) for MFD1 and MFD2, respectively. The differences between the average values of $\beta\Xi$ for MFD1 and MFD2 and the exact value of $\beta\Xi$ [43,48] are less than 1%. Arrows indicate the exact values of $\beta\Xi$ and the lines are from the fitted asymptotic behavior of $\Lambda(H)$ in the SD region.

exact values [43,48] 4.942, 4.004, and 3.217, respectively.

Since the nucleation rate for a single droplet is independent of the system size, the average metastable lifetime in the SD region should be proportional to $L^{-2}$, as indicated by Eq. (27). We checked this result at $T$=1.0 and $|H|^{-1}$=2.47 by fitting the lifetime to the form $\langle\tau\rangle\propto L^{-\alpha}$ for $L$=12, 14, 16, 20, and 24 (in the SD region for all the values of $L$ used). From this we obtained $\alpha$=2.08(3), in reasonable agreement with the theoretical result. At higher temperatures the agreement is less convincing, so that at $0.8T_c$ we found $\alpha\approx 3$ for the same values of $L$. However, we believe this is a finite-size effect that becomes more pronounced at higher temperatures.

It is also possible to construct mean-field dynamics that interpolate smoothly between MFD1 and MFD2. In analogy to Eqs. (8) and (11) the transition probabilities of such a dynamic can be written as

$$W_\gamma(n,n+1) = A\left(1-\frac{n}{N}\right)^\gamma \exp\left(\min\left\{0,\{F(n) - F(n+1) + \gamma[S(n) - S(n+1)]\}\right\}\right), \tag{37a}$$

$$W_\gamma(n,n-1) = A\left(\frac{n}{N}\right)^\gamma \exp\left(\min\left\{0,\{F(n) - F(n-1) + \gamma[S(n) - S(n-1)]\}\right\}\right), \tag{37b}$$

$$W_\gamma(n,n) = 1 - W_\gamma(n,n+1) - W_\gamma(n,n-1)\ . \tag{37c}$$

The positive constant $A$ only needs to fulfill the requirement that $W_\gamma(n,n) \geq 0$ for all $n$, and it is otherwise unimportant since it only redefines the overall time scale of the process. In principle, the only restriction on $\gamma$ should be $\gamma \geq 0$. For $\gamma$=1 and $A$=1 the process reduces to MFD1, while for $\gamma$=0 and $A$=1/2 it reduces to MFD2. Since both the prefactors $b$+$c$ in the SD region and the $L$ dependence for the low-temperature strong-field behavior of $H_{\rm DSP}$ are different for MFD1 and MFD2, it is expected that they both change continuously with $\gamma$. Thus it may be possible to tailor a mean-field dynamic to give the desired prefactor and $H_{\rm DSP}$ dependence to match a particular microscopic dynamic. For MC simulations with sites selected sequentially, MFD1 has the desired values of these two quantities. If $\gamma$=1/2, then the $T$ dependence of $H_{\rm DSP}$ will be given by Eq. (36c), which agrees with MC simulations with randomly selected sites. The mean-field dynamic with $\gamma$=1/2 might also be expected to give a prefactor closer to the value for MC simulations with randomly selected sites, $b$+$c$=3 [5], since this lies between the values we have obtained for MFD1 and MFD2.

In Fig. 9, we show $T\Lambda$ for the very low temperatures $T$=0.4, 0.2, and 0.1. Discrete-droplet results for low $T$ [58–63] are shown as a set of parabolic arcs given by Eq. (34). For $T$=0.4 we observe clear oscillatory behavior with $|H|$, even though quantitative agreement with the discrete-droplet limit has not set in yet. For $T$=0.2 and 0.1 we observe increasingly good quantitative agreement between the MFD1 results and the discrete-droplet limit. For $T$=0.4, $\langle\tau\rangle$ is on the order of $10^7$ and $10^{26}$ for $|H|$=1.0 and $|H|$=0.3, respectively, as obtained from MFD1 with

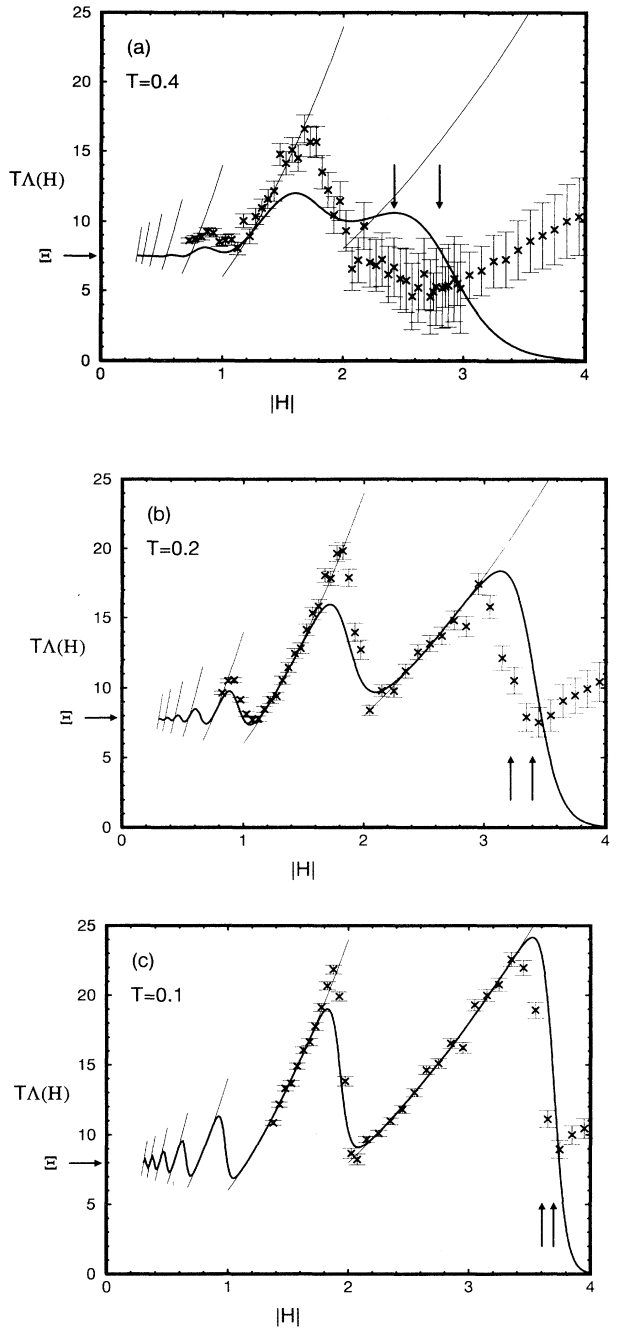


FIG. 9. (a) The field dependence of $T\Lambda(H)$ for MFD1 at $T$=0.4. The discrete-droplet [58–63] result is shown as a set of parabolic arcs. The exact value of $\Xi$ [43,48] is indicated by the horizontal arrow. Simulation results for $L$=24 [6] from the Metropolis algorithm with spin updates at randomly chosen sites and $10^3$ escapes from the initial state are also shown. The two vertical arrows indicate the estimates of $H_{1/2}$ from MC simulation (left) and MFD1 (right). (b) Same as (a) at $T$=0.2. The results from the MC simulations and MFD1 agree quite well with the discrete-droplet [58–63] result. (c) Same as (a) at $T$=0.1. The agreement between the three sets of results is close. Here the relaxation time $\langle\tau\rangle$ from MFD1 with $m_{\rm cut}$=0 is on the order of $10^{39}$ and $10^{123}$ at $|H|$=1.0 and 0.3, respectively. The MC estimate for $\langle\tau\rangle$ is on the order of $10^{31}$ at $|H|$=1.35.

$m_{\rm cut}$=0. The corresponding numbers for $T$=0.2 (0.1) are $10^{18}$ ($10^{39}$) and $10^{59}$ ($10^{123}$).

MC results by one of us [6] provide corroboration for the MFD1 results. This oscillatory behavior with $|H|$ is due to the corrugation of the free energy near the saddle point, illustrated in Fig. 1(b). This corrugation is due to the discreteness of the lattice.

## VI. RELATIONS TO EARLIER WORK

The relationships of the detailed shape of $F(m)$ to two-phase equilibria and nucleation barriers in finite systems have previously been studied by Schulman [3] and by Binder and co-workers [18–20]. Since $F(m)$ can be viewed as a potential for the stochastic processes that define our macroscopic dynamics [3], it might have been expected that those studies would have also revealed two $L$-dependent spinodals with the same scaling behaviors as $H_{\rm THSP}$ and $H_{\rm DSP}$. However, Furukawa and Binder instead reported a single spinodal at a field proportional to $L^{-1}$ [19].

To clarify the relation between our results and those of these earlier studies, we follow Refs. [3,19] by calculating

$$h(m) = (\beta L^d)^{-1} \frac{dF_0(m)}{dm} \ . \tag{38}$$

This quantity has the dimension of a field and is the equivalent, for an Ising model in the fixed-$m$ ensemble, of the expectation value of the chemical potential for a lattice gas in the fixed-density ensemble [19]. In Fig. 10 we show $h(m)$ for $L$=24, 32, 64, and 96 at $0.8T_c$ [68]. (For $L$=96 the simulation was only performed for $|m|>0.63$.) From Eqs. (1) and (38) it is seen that

$$\frac{dF(m)}{dm} = \beta L^d \left[h(m) - H\right] \ . \tag{39}$$

Thus the extrema of the field-dependent $F(m)$ occur where the applied field $H$ equals $h(m)$. For a negative $H$ between zero and the minimum of $h(m)$, there are three such extrema: the stable minimum at $m \approx -m_{\rm eq}(T)$, the metastable minimum at $m \approx +m_{\rm eq}(T)$, and an unstable maximum at some $m$ between 0 and $m_{\rm sp}$, the magnetization corresponding to the minimum of $h(m)$. If dynamically relevant information for nonzero $H$ is to be deducible from the functional form of $F(m)$, this must mean that the spatial configuration characteristic of the nonequilibrium saddle point of the relaxing system is well approximated by the *equilibrium* configuration corresponding to the same value of $m$ in the fixed-$m$ ensemble. It is not unreasonable to expect that this should hold, at least for sufficiently large systems, where the corresponding applied $H$ is weak.

Following the reasoning outlined above, we start by considering the thermodynamic spinodal. The droplet-theoretical arguments in Sec. IV indicate that the THSP should be located in the field range where $R_c$ becomes on the order of $L$, so that the droplet must compete with slab configurations to become the "true" saddle point. It has been shown by Leung and Zia [42] that for Ising models with periodic boundary conditions in the fixed-$m$ ensemble, a first-order phase transition between the equilibrium droplet and slab configurations occurs at a temperature dependent magnetization, $m_c(T)$. For $|m|<m_c$ the equilibrium configuration is a slab. The volume fraction corresponding to $m_c(T)$ in the limit $L \to \infty$, which was obtained in Ref. [42], can be written as [49]

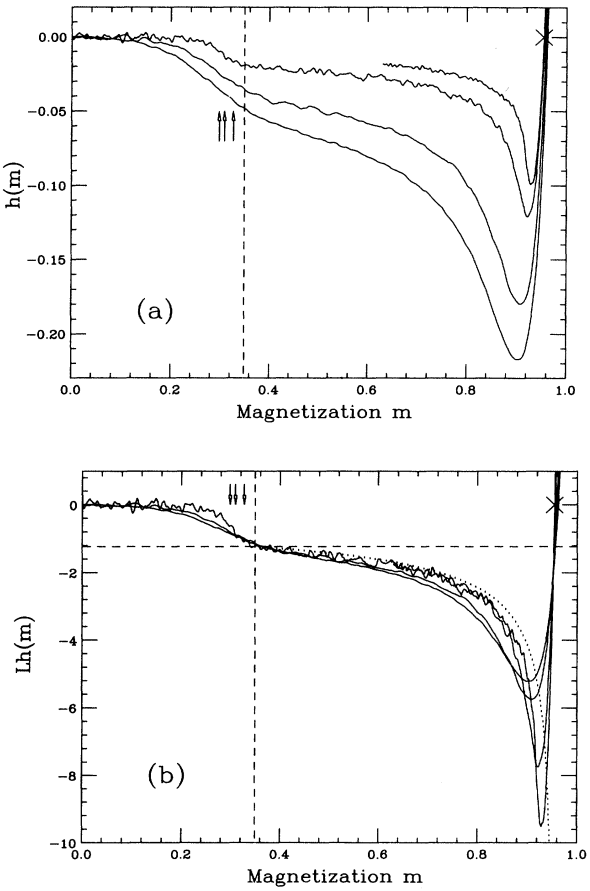


FIG. 10. The quantity $h(m)$, defined in Eq. (38), shown vs magnetization $m$ at $T$=$0.8T_c$. The large × marks the spontaneous zero-field magnetization at this temperature. For detailed discussion, see Sec. VI. The vertical, dashed line in both panels marks $m_c$, corresponding to the droplet-to-slab transition in the limit $L \to \infty$, and the vertical arrows mark $m_c$ for the three smallest $L$ studied (from left to right). (a) Shows $h(m)$, highlighting the developing step discontinuity near $m_c$, related to the thermodynamic spinodal, and the narrow minimum near $m_{\rm sp}$, related to the dynamic spinodal. From bottom to top the system sizes are $L$=24, 32, 64, and 96 (the latter only for $m>0.63$). (b) Shows $L\,h(m)$, highlighting the $L^{-1}$ scaling behavior of $h(m)$ in the SD region between $m_c$ and $m_{\rm sp}$, as well as the much slower vanishing of the minimum value, $h(m_{\rm sp})$. The horizontal, dashed line corresponds to $L\,H_{\rm THSP}$ from Eq. (41), and the dotted curve is the asymptotic single-droplet result for $L\,h(m)$ obtained by applying Eq. (38) to $F_0^{(1)}$ from Eq. (42a).

$$\phi_c(T) = \left(\frac{2\sigma_0(T)}{d}\right)^{\frac{d}{d-1}} \left(\frac{d-1}{2m_{\rm eq}(T)}\right) [\Xi(T)]^{-\frac{1}{d-1}} . \quad (40)$$

The vertical, dashed lines in Fig. 10 mark $m_c(0.8T_c)$. If one ignores entropy effects due to the center-of-mass positions of the droplet and slab, as well as capillary waves on their surfaces (which are responsible for the $|H|^b$ power-law prefactor in the nucleation rate [17]), the finite-size displacement of $m_c$ is proportional to $L^{-1}$ [42]. The vertical arrows in Fig. 10 indicate the corresponding values of $m_c$ for $L$=24, 32, and 64, as obtained from Fig. 3 of Ref. [42]. These values monotonically approach the infinite-$L$ limit for $m_c$. From Fig. 10(a) it appears that the shape of $h(m)$ evolves towards a step discontinuity as $L$ increases. From the data collapse in the plots of $Lh(m)$ in Fig. 10(b), it is seen that the magnitude of this discontinuity is proportional to $L^{-1}$ and so corresponds to a finite discontinuity in a first derivative of the free energy per unit interface area, $L^{-(d-1)}F_0(m)$, in the fixed-$m$ ensemble. This is consistent with the identification of the droplet-to-slab transformation as a first-order phase transition [42].

Using $\phi_c(T)$ from Eq. (40) in Eq. (25) for $H_{\rm THSP}(\phi)$, we obtain an estimate for $H_{\rm THSP}$ as the field at which the free energies of the critical droplet and a system-spanning slab are degenerate:

$$H_{\rm THSP} = H_{\rm THSP}(\phi_c) = \frac{1}{L}\left(\frac{d\,\Xi(T)}{2\sigma_0(T)}\right)^{\frac{1}{d-1}} . \quad (41)$$

The horizontal, dashed line in Fig. 10(b) represents this estimate of $L\,H_{\rm THSP}$. It corresponds excellently to the magnitude of the incipient step discontinuity in $L\,h(m)$. The $L$ dependence of $H_{\rm THSP}$ at $0.8Tc$ is shown in Fig. 11, together with the results of MFD1 for $L$=32 and 64. The MFD1 points were estimated as the smallest fields for which $\Lambda(T,H)=\beta\Xi(T)$ (see Fig. 4). The agreement is good and we believe the small discrepancy is a finite-size effect.

The narrow minimum in $h(m)$, which occurs at an $L$-dependent magnetization $m_{\rm sp}(L)$, slightly smaller than the equilibrium magnetization $m_{\rm eq}$, signifies the inflection point in $F_0(m)$. This magnetization also corresponds to a change in the equilibrium configuration: the system is uniform closer to $m_{\rm eq}$, whereas closer to $m_c$ a single droplet of the opposite magnetization is precipitated [3,19]. The volume fraction occupied by this droplet is given by the lever rule. As seen from Fig. 10(b), the minimum value of $h(m)$, $h(m_{\rm sp})$, does not vanish as $L^{-1}$.

It is tempting to identify the disappearance of the single-droplet saddle point, which occurs at $h(m_{\rm sp})$, with the dynamic spinodal, $H_{\rm DSP}$. For all the system sizes studied here, we find that $|h(m_{\rm sp})|$ indeed lies close to other estimates for $H_{\rm DSP}$, such as $H_{1/2}$ obtained both from MFD1 and from microscopic MC simulations. These comparisons are illustrated in Fig. 11. Obviously, the range of $L$ used in the present study is too narrow to obtain the scaling relation with any degree of certainty. However, the values of $|h(m_{\rm sp})|$ at different $L$ also agree well with the estimate for $H_{\rm DSP}$ obtained in Ref. [5] by

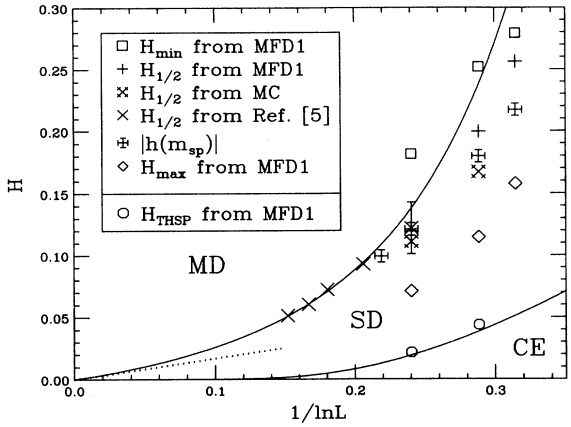


FIG. 11. "Spinodal phase diagram," showing the MD, SD, and CE regions in the $(1/\ln L,\ H)$ plane for the two-dimensional Ising model at $0.8T_c$. The lower, solid curve is $H_{\rm THSP}$ from Eq. (41), and the data points (○) close to it are $H_{\rm THSP}$ from MFD1 for $L$=32 and 64. The upper, solid curve is $H_{\rm DSP}$ from Ref. [5], obtained from a one-parameter fit of the relation $L\propto R_0$ to MC data for $L$=64, 128, 256, 400, and 720. The short, dotted line indicates the asymptotic slope of $H_{\rm DSP}$. The data points represent different estimates for $H_{\rm DSP}$, obtained from MFD1, MC simulations in this work, $|h(m_{\rm sp})|$, and from MC simulations for larger systems in Ref. [5], as indicated by the key in the figure. The quantities in the upper box are all estimates for $H_{\rm DSP}$. In all cases, error bars are only given where the statistical error is larger than the symbol size. From right to left the data points correspond to $L$=24, 32, 64, 96, 128, 256, 400, and 720. See detailed discussion in Sec. VI.

fitting the proportionality constant in the relation $L\propto R_0$ with $R_0$ given by Eq. (31) to MC data for $L$ between 64 and 720. We find this noteworthy, considering that this analytical expression for $H_{\rm DSP}$ is based on explicitly dynamical arguments, whereas $|h(m_{\rm sp})|$ is obtained from a strictly equilibrium calculation.

To account for this observation, we suggest that $m_{\rm sp}$ corresponds to the volume fraction at which entropy effects make the free energy of a configuration consisting of multiple droplets lower than that of the single-droplet configuration. We assume that the single droplet is replaced by two identical droplets, each with half the volume of the original droplet. We neglect corrections to the droplet free energy, including those arising from surface excitations, which correspond to the power-law prefactor $|H|^b$ in Eq. (26). We only consider the entropy contributions due to the droplets' center-of-mass positions, and we neglect excluded-volume effects. This gives the approximate zero-field free energies

$$F_0^{(1)}(\phi) \approx F_0(m_{\rm eq}(T)) + L^{d-1}d\beta\left(\frac{2m_{\rm eq}(T)\phi}{d-1}\right)^{\frac{d-1}{d}} \times[\Xi(T)]^{\frac{1}{d}} - d\ln L \quad (42a)$$

for the single-droplet configuration and

$$F_0^{(2)}(\phi) \approx F_0(m_{\rm eq}(T)) + 2^{\frac{1}{d}} L^{d-1} d\beta \times \left(\frac{2m_{\rm eq}(T)\phi}{d-1}\right)^{\frac{d-1}{d}} [\Xi(T)]^{\frac{1}{d}} - 2d\ln L \quad (42b)$$

for the two-droplet configuration. Equating $F_0^{(1)}$ and $F_0^{(2)}$ we find

$$\phi_{\rm sp} \approx \frac{d-1}{2m_{\rm eq}(T)[\Xi(T)]^{\frac{1}{d-1}} L^d} \left(\frac{T\ln L}{2^{\frac{1}{d}}-1}\right)^{\frac{d}{d-1}} . \quad (43)$$

Inserting $\phi_{\rm sp}$ into the single-droplet approximation for $|h(\phi)|$ obtained from $F^{(1)}$ through Eq. (38), which is identical to the expression for $H_{\rm THSP}(\phi)$ given in Eq. (25), we obtain

$$|h(\phi_{\rm sp})| \approx \left(\frac{(2^{\frac{1}{d}}-1)\beta\Xi(T)}{\ln L}\right)^{\frac{1}{d-1}} . \quad (44)$$

Comparing this result with Eq. (32) for $H_{\rm DSP}$ we note that, except for a $d$-dependent numerical constant of order unity, it has the same asymptotic dependences on $L$ and $T$ as $H_{\rm DSP}$. In particular, $|h(\phi_{\rm sp})|$ does *not* vanish as $L^{-1}$, but rather much more slowly as $(\ln L)^{-\frac{1}{d-1}}$. As noted previously and illustrated in Fig. 11, corrections to this asymptotic behavior for $H_{\rm DSP}$, due to the power-law prefactors in the nucleation rate, are very substantial. Since analogous corrections were ignored in the approximate derivation of $|h(\phi_{\rm sp})|$ given here, we expect similarly large corrections to apply to it. This is in agreement with the numerical results shown in Figs. 10 and 11. We further note that the precise value of the numerical coefficient in our approximate expression for the asymptotic value of $|h(\phi_{\rm sp})|$ is the result of our choice to consider only a separation of the single droplet into two *equal* droplets. A more careful calculation ought, therefore, to give a different coefficient. However, the factor $(d+1)$ in the denominator of $H_{\rm DSP}$ results specifically from the simultaneous nucleation and growth processes that give rise to the expression for the lifetime in the MD region, Eq. (29). It is, therefore, unlikely that further improvement of the equilibrium calculation should yield the same factor in $|h(\phi_{\rm sp})|$. Comparing the single-droplet free energy directly with that of a uniform phase, ignoring entropy effects, one gets $\phi_{\rm sp} \propto L^{-\frac{d}{d+1}}$ [3] and $|h(\phi_{\rm sp})| \propto L^{-\frac{d}{d+1}}$. This result agrees less well with our numerical data than does the $L$ dependence in Eqs. (43) and (44).

For $|H|>|h(m_{\rm sp})|$ the bulk free energy displays no saddle point, but its derivative with respect to $m$ has a minimum at $m_{\rm sp}$. As a consequence, mean-field dynamics should show a slowing down near $m_{\rm sp}$, as observed in the present study. However, $F(m)$ does not contain information about the complicated multidroplet configurations that dominate the dynamics in this region of relatively strong fields. Consequently, we expect the agreement between microscopic and mean-field dynamics to be only qualitative in the MD region.

## VII. DISCUSSION

In this paper, we have introduced a class of macroscopic mean-field dynamics and have studied in detail two members of this class, which we call MFD1 and MFD2. We have demonstrated that these macroscopic mean-field dynamics replicate many of the qualitative and quantitative features of the relaxation behavior of the metastable phase of the two-dimensional nearest-neighbor Ising model. As a function of the external field $H$, four distinct regions of relaxation were observed in agreement with recent microscopic MC studies [1,5]. In the single-droplet region at low temperatures, the leading exponential term in the relaxation time $\langle\tau\rangle$ was obtained to within 1% of the exact value. We also obtained temperature independent estimates for the prefactor exponents $b+c$ for the two mean-field dynamics. At very low temperatures we observed an oscillatory behavior in $\Lambda(H)\equiv d\ln\langle\tau\rangle/d|H|^{-1}$ with respect to $|H|$, in agreement with discrete-droplet theory. In the low-temperature limit, simple theoretical estimates of the dynamic spinodal field $H_{\rm DSP}$, in terms of the temperature and the system size, were obtained for various dynamics. Our numerical studies provide excellent agreement with these predictions.

The mean-field dynamics are constructed with only the following conditions: (1) locality in the value of the order parameter $m$ and (2) the correct equilibrium distribution obtained from the order parameter of the microscopic model. These two conditions constitute the minimum requirements for any local dynamic. The reasonable results obtained from the macroscopic mean-field dynamics may be somewhat surprising in view of the fact that no microscopic information is directly included. However, we believe the relative success of our dynamics becomes more understandable if one views them as approximations to the macroscopic dynamic that can formally be constructed by using a projection-operator formalism to project the microscopic dynamic onto a master equation for the one-dimensional order-parameter distribution, as discussed in Appendix A. The dynamically relevant information that is retained in $F(m)$ following this projection correctly describes the droplet configurations that provide the rate-determining steps in the decay process. In particular, these are the droplet and slab configurations that are important near the thermodynamic spinodal, the single-droplet configuration characteristic of the SD region, and the breakdown of the single-droplet configuration into a uniform "gas" of microscopic fluctuations that takes place near the dynamic spinodal. These aspects were discussed in light of earlier work in Sec. VI. As a consequence, the mean-field dynamics produce excellent numerical estimates for both the thermodynamic and the dynamic spinodal fields.

Comparison between the two proposed dynamics, MFD1 and MFD2, provides some insight into the dependence of the lifetime $\tau$ on the detailed dynamics. Most of the characteristic behavior of $\Lambda$ predicted by both continuous- and discrete-droplet theory [5,58] is expected to hold for different local dynamics. However, the influence of the detailed dynamic is reflected in the prefactor exponent $b+c$. The difference between $\Lambda(H)$ as obtained from MFD1 and MFD2 in the deterministic region suggests that $\Lambda(H)$ in this region depends strongly on the particular dynamic.

Generally, when the relaxation time is long, the system spends more time exploring phase space, and, therefore, the dynamic is more strongly subject to the restricted bulk free energy $F(m)$, as indicated in this study. When the relaxation time is short, the details of the particular dynamic are more important than the bulk free energy. From the field-theoretical point of view, when the most probable trajectory from the metastable phase to the unstable saddle point is sharply defined, the relaxation time is usually large, and regardless of the details of the particular dynamic, one needs to consider only the trajectories near the most probable one in order to study the decay of the metastable phase. When the probability distribution over trajectories is not very sharp, the lifetimes are usually short and the details of the particular dynamic play important roles.

The biggest advantage of macroscopic mean-field dynamics is that they can provide data for low temperatures and weak fields (in the single-droplet region), for which the average lifetime of the metastable phase is too long to be measured with standard MC algorithms. They also provide data for arbitrary temperatures and fields, allowing one to obtain accurate estimates of derivatives. However, the system sizes for which mean-field dynamics can be applied are rather limited by computational constraints.

In summary, we have presented a method to study the relevance of the equilibrium properties of a model to the dynamical relaxation of metastable phases. The macroscopic dynamics are designed using only the minimal requirements of locality in the relevant order parameter and the correct equilibrium free energy projected on that order parameter. Extensive applications to the two-dimensional nearest-neighbor Ising ferromagnet on a square lattice provides convincing evidence that the characteristic behavior of the dynamical relaxation of the metastable phases is largely determined by the restricted bulk free energy $F(m)$. We believe that our approach can benefit studies of relaxation phenomena for other systems as well.

## ACKNOWLEDGMENTS

We would like to thank K. Binder, M. Grant, J. M. Kosterlitz, H. Tomita, and J. Viñals for useful discussions, and B. M. Gorman, C. C. A. Günther, R. A. Ramos, H. L. Richards, and S. W. Sides for helpful comments on the manuscript. This work was supported in part by Florida State University through the Supercomputer Computations Research Institute (U.S. Department of Energy Contract No. DE-FC05-85ER25000). P.A.R. is also supported by National Science Foundation Grant No. DMR-9315969 and by the Florida State University Center for Materials Research and Technology (MARTECH).

## APPENDIX A: RELATION OF OUR MACROSCOPIC MAGNETIZATION DYNAMICS TO THE MICROSCOPIC SPIN DYNAMIC

In this appendix, we briefly consider the formal relationship between our macroscopic magnetization dynamics, MFD1 and MFD2, and the underlying microscopic dynamic represented by the single-spin-flip Metropolis algorithm with updates at randomly selected sites. The formal framework for the discussion is the Nakajima-Zwanzig [25,26] projection-operator formalism for the master equation, which is equivalent to Mori's [27] projection-operator formalism for the equations of motion of observables [28,29]. We adapt the standard discussion (see, e.g., Refs. [29,30]), which considers a deterministic microscopic dynamic governed by a quantum-mechanical or classical Hamiltonian, to the case where the microscopic dynamic is a discrete-time Markov process (possibly derived from a deterministic dynamic at an even more microscopic level).

For an $N$-site kinetic Ising model, the microscopic probability density at time $k$ is a $2^N$-dimensional column vector $\vec{\rho}(k)$ which evolves in time according to the equation

$$\vec{\rho}(k+1) = \mathcal{W}\vec{\rho}(k) \ , \tag{A1}$$

where $\mathcal{W}$ is the matrix of microscopic transition probabilities. The probability distribution over the "relevant" macroscopic variables at time $k$, $\vec{X}(k)$, is obtained from $\vec{\rho}(k)$ through the action of a projection operator $\mathcal{P}$,

$$\vec{X}(k) = \mathcal{P}\vec{\rho}(k) \ . \tag{A2}$$

Although the dimension of $\vec{X}(k)$ is $2^N$, if the only macroscopic variable considered is the magnetization, the dimension of the "relevant" space in which $\vec{X}(k)$ has nonzero components is $N+1$. By using Eqs. (A1) and (A2), one can write the equation of motion for $\vec{X}(k)$ as

$$\begin{aligned}\vec{X}(k+1) &= \mathcal{P}\mathcal{W}\vec{\rho}(k) = \mathcal{P}\mathcal{W}(\mathcal{P}+\mathcal{Q})\vec{\rho}(k) \\ &= \mathcal{P}\mathcal{W}\vec{X}(k) + \mathcal{P}\mathcal{W}\left[\mathcal{Q}\vec{\rho}(k)\right] \ ,\end{aligned} \tag{A3}$$

where $\mathcal{Q}=\mathbf{1}-\mathcal{P}$ is the projection operator onto the "irrelevant" orthogonal complement to the relevant space. The first term in the second line of Eq. (A3) corresponds to a Markov process for $\vec{X}(k)$, whereas the second term contains non-Markov contributions that can be formally evaluated as follows.

Operating on Eq. (A1) with $\mathcal{Q}$ one obtains

$$\begin{aligned}\mathcal{Q}\vec{\rho}(k) &= \mathcal{Q}\mathcal{W}\vec{\rho}(k-1) = \mathcal{Q}\mathcal{W}(\mathcal{P}+\mathcal{Q})\vec{\rho}(k-1) \\ &= \mathcal{Q}\mathcal{W}\vec{X}(k-1) + \mathcal{Q}\mathcal{W}\left[\mathcal{Q}\vec{\rho}(k-1)\right] \ ,\end{aligned} \tag{A4}$$

which is inserted in Eq. (A3). Iterating this procedure a total of $k$ times, one obtains the final result,

$$\begin{aligned}\vec{X}(k+1) = \mathcal{P}\mathcal{W}\vec{X}(k) &+ \mathcal{P}\mathcal{W}\sum_{l=1}^{k}\left[\mathcal{Q}\mathcal{W}\right]^l\vec{X}(k-l) \\ &+\mathcal{P}\mathcal{W}\left[\mathcal{Q}\mathcal{W}\right]^k\mathcal{Q}\vec{\rho}(0) \ .\end{aligned} \tag{A5}$$

The first term on the right-hand side corresponds to a Markov process in the relevant subspace. The non-Markovian second and third terms represent memory about the relevant variables at earlier times, propagated

through the irrelevant subspace, and specific information about the initial state of the irrelevant variables, respectively [30]. The third term can usually be ignored, at least after a short initial period.

In standard applications of projection-operator techniques, the quality of the resulting approximation depends on the choice of the relevant macroscopic variables. The approach is most useful whenever there is a large separation between "fast" and "slow" time scales, and one usually attempts to include all the slow variables in the relevant subspace. This ensures that only variables with short correlation times contribute to the memory effects, which can then often be ignored or approximated by a rapidly decaying function. The (most obvious) slow variables are determined by macroscopic conservation laws or by spontaneously broken symmetries in the corresponding isolated system [29].

In the present work, we have considered the stochastic time evolution of the magnetization (our relevant macroscopic variable) as a Markov process defined by the transition probability matrices $\mathbf{W}_1$ (for MFD1) or $\mathbf{W}_2$ (for MFD2). In doing so, we have performed a Markov approximation equivalent to ignoring the memory effects and using $\mathbf{W}_1$ and $\mathbf{W}_2$ as approximations for the matrix obtained by contracting $\mathcal{PW}$ in Eq. (A5), so that its dimension becomes $N+1$. The macroscopic slowness of the magnetization is related to the spontaneously broken symmetry between the two ferromagnetic phases for $H=0$ below $T_c$. By virtue of energy conservation in the corresponding closed system, the other obvious slow macroscopic variable is the total energy. In relegating it to the irrelevant subspace, mainly for computational convenience, we have most likely ignored non-negligible memory effects. By considering only a single relevant variable we also have excluded nonlinear interactions between macroscopic variables [29].

The satisfactory agreement between our approximate macroscopic Markovian dynamics and the MC simulations of the full microscopic dynamic indicates that the approximations made in the present work are quite reasonable. Nevertheless, the above discussion indicates that by including the total energy as a second relevant macroscopic variable in our Markovian mean-field dynamics, we could reduce the importance of the neglected memory effects and allow for nonlinear interactions between relevant variables. We believe further significant improvement of the agreement between the approximate, macroscopic dynamics and the underlying microscopic dynamic could be achieved in this way.

## APPENDIX B: ABSORBING MARKOV CHAINS

In this appendix, we briefly discuss the application of absorbing Markov chains [32] to obtain the expectation value and the variance of the first-passage time for escape from the metastable phase. For a given transition probability matrix $W(n,n')$, simple matrix calculations provide the expectation value and the standard deviation of the first-passage time from one state to another.

Let us consider a random walker that moves between states $0 \le n,n' \le N$ with transition probabilities $W(n,n')$. Starting from an arbitrary initial state $\vec{X}(0)$, the probability density after $k$ time steps, $\vec{X}(k)$, is

$$\vec{X}(k) = \mathbf{W}^k \vec{X}(0) \; . \tag{B1}$$

Without absorbing states, the probability of a Markov chain is conserved, that is,

$$\sum_{n'} W(n,n') = 1 \tag{B2}$$

for all $n$. After $k$ time steps the walker is still in some state, that is,

$$\vec{e}^{\,\mathrm{T}} \mathbf{W}^k \vec{X}(0) = 1 \; , \tag{B3}$$

where $\vec{e}^{\,\mathrm{T}} = (1,\ldots,1,\ldots,1)$ and the superscript T denotes the transpose.

Now we place absorbing states at $i \ge n_{\mathrm{cut}}$. Once an absorbing state is reached, the walker is absorbed and the Markov chain terminates. Let $\mathbf{T}$ be the $n_{\mathrm{cut}} \times n_{\mathrm{cut}}$ submatrix of $\mathbf{W}$ that contains the transition probabilities between the $n_{\mathrm{cut}}$ transient states. The analog of Eq. (B2) is not satisfied for $\mathbf{T}$. The probability that the walker is absorbed at time $k$ is $\vec{e}^{\,\mathrm{T}}(\mathbf{T}^{k-1} - \mathbf{T}^k)\vec{X}(0)$. The average first-passage time to the absorbing states is

$$\langle \tau \rangle = \sum_{k=1}^{\infty} \vec{e}^{\,\mathrm{T}} k(\mathbf{T}^{k-1} - \mathbf{T}^k)\vec{X}(0) = \vec{e}^{\,\mathrm{T}} \mathbf{N} \vec{X}(0) \; . \tag{B4}$$

The fundamental matrix is defined by $\mathbf{N} = (\mathbf{I} - \mathbf{T})^{-1}$, where $\mathbf{I}$ is the identity matrix. Similarly, the second moment of the first-passage time can be obtained from [32]

$$\langle \tau^2 \rangle = \vec{e}^{\,\mathrm{T}} (2\mathbf{N}^2 - \mathbf{N})\vec{X}(0) \; . \tag{B5}$$

In this work, $\tau$ was divided by the total number of sites $N$, so that all times are given in units of MCSS.


[1] P. A. Rikvold and B. M. Gorman, in *Annual Reviews of Computational Physics I*, edited by D. Stauffer (World Scientific, Singapore, 1994), p. 149.

[2] O. Penrose and J. L. Lebowitz, J. Stat. Phys. **3**, 211 (1971); in *Fluctuation Phenomena*, edited by E. W. Montroll and J. L. Lebowitz (North-Holland, Amsterdam, 1979), Chap. 5, p. 293.

[3] L. S. Schulman, J. Phys. A **13**, 237 (1980); in *Finite-size Scaling and Numerical Simulation of Statistical Systems*, edited by V. Privman (World Scientific, Singapore, 1990), p. 489.

[4] H. Tomita and S. Miyashita, Phys. Rev. B **46**, 8886 (1992).

[5] P. A. Rikvold, H. Tomita, S. Miyashita, and S. W. Sides, Phys. Rev. E **49**, 5080 (1994).

[6] M. A. Novotny, Phys. Rev. Lett. **74**, 1 (1995).

[7] M. E. Fisher, Physics (Long Island City, NY) **3**, 255 (1967).

[8] J. S. Langer, Ann. Phys. **41**, 108 (1967).

[9] J. S. Langer, Phys. Rev. Lett. **21**, 973 (1968).

[10] J. S. Langer, Ann. Phys. **54**, 258 (1969).
[11] C. C. A. Günther, P. A. Rikvold, and M. A. Novotny, Phys. Rev. Lett. **71**, 3898 (1993).
[12] C. C. A. Günther, P. A. Rikvold, and M. A. Novotny, Physica A **212**, 194 (1994).
[13] P. A. Rikvold, B. M. Gorman, and M. A. Novotny, in *Slow Dynamics in Condensed Matter*, edited by K. Kawasaki, M. Tokuyama, and T. Kawkatsu, AIP Conf. Proc. No. 256 (AIP, New York, 1992), p. 549.
[14] B. M. Gorman, P. A. Rikvold, and M. A. Novotny, Phys. Rev. E **49**, 2711 (1994).
[15] T. Fiig, B. M. Gorman, P. A. Rikvold, and M. A. Novotny, Phys. Rev. E **50**, 1930 (1994).
[16] P. A. Rikvold, Prog. Theor. Phys. Suppl. **99**, 95 (1989); Phys. Scr. **T38**, 36 (1991).
[17] N. J. Günther, D. A. Nicole, and D. J. Wallace, J. Phys. A **13**, 1755 (1980).
[18] K. Binder and M. H. Kalos, J. Stat. Phys. **22**, 363 (1980).
[19] H. Furukawa and K. Binder, Phys. Rev. B **26**, 556 (1982).
[20] K. Kaski, K. Binder, and J. D. Gunton, Phys. Rev. B **29**, 3996 (1984).
[21] P. C. Hohenberg and B. Halperin, Rev. Mod. Phys. **49**, 435 (1977).
[22] R. B. Griffiths, C.-Y. Weng, and J. S. Langer, Phys. Rev. **149**, 301 (1966).
[23] N. Metropolis, A. W. Rosenbluth, M. N. Rosenbluth, A. H. Teller, and E. Teller, J. Chem. Phys. **21**, 1087 (1953).
[24] See, e.g., K. Binder, in *Monte Carlo Methods in Statistical Physics*, edited by K. Binder (Springer, Berlin, 1986), p. 5.
[25] S. Nakajima, Prog. Theor. Phys. **20**, 948 (1958).
[26] R. Zwanzig, J. Chem. Phys. **33**, 1338 (1960).
[27] H. Mori, Prog. Theor. Phys. **33**, 423 (1965).
[28] H. Grabert, Z. Phys. B **26**, 79 (1977).
[29] H. Grabert, *Projection Operator Techniques in Nonequilibrium Statistical Mechanics* (Springer, Berlin, 1982), and references cited therein.
[30] S. Nordholm and R. Zwanzig, J. Stat. Phys. **13**, 347 (1975).
[31] J. Lee and J. M. Kosterlitz, Phys. Rev. Lett. **65**, 137 (1990).
[32] M. Iosifescu, *Finite Markov Processes and Their Applications* (Wiley, New York, 1980), p. 99.
[33] Note that, in contrast to the notation in Ref. [5], in the present work the Hamiltonian is *not* divided by $T$. Therefore, the definitions of some quantities are different from those in Ref. [5]. The notation used in this work is consistent with Refs. [1,6,11,12].
[34] J. P. Valleau and D. N. Card, J. Chem. Phys. **57**, 5457 (1972).
[35] G. M. Torrie and J. P. Valleau, J. Comput. Phys. **23**, 187 (1977); J. Chem. Phys. **66**, 1402 (1977).
[36] M. H. Kalos and P. A. Whitlock, *Monte Carlo Methods I* (Wiley, New York, 1986), Chap. 3.7.
[37] A. Hüller, Z. Phys. B **88**, 79 (1992).
[38] B. A. Berg and T. Neuhaus, Phys. Lett. B **267**, 249 (1991); Phys. Rev. Lett. **68**, 9 (1992).
[39] B. A. Berg and T. Celik, Phys. Rev. Lett. **69**, 2292 (1992); B. A. Berg, Int. J. Mod. Phys. C **3**, 1083 (1992).
[40] B. A. Berg, U. Hansmann, and T. Neuhaus, Phys. Rev. B **47**, 497 (1993).
[41] J. Lee, Phys. Rev. Lett. **71**, 211 (1993); **71**, 2353(E) (1993).
[42] K. Leung and R. K. P. Zia, J. Phys. A **23**, 4593 (1990).
[43] R. K. P. Zia and J. E. Avron, Phys. Rev. B **25**, 2042 (1982).
[44] C. N. Yang, Phys. Rev. **85**, 808 (1952).
[45] K. Binder, Z. Phys. B **43**, 119 (1981).
[46] K. Binder, Phys. Rev. A **25**, 1699 (1982).
[47] B. Berg, U. Hansmann, and T. Neuhaus, Z. Phys. B **90**, 229 (1993).
[48] C. Rottman and M. Wortis, Phys. Rev. B **24**, 6274 (1981).
[49] Our quantity $\Xi(T)$ is identical to $[(d-1)/2m_{\rm eq}(T)]^{d-1}W(T)$, where $W$ is the quantity defined in Eq. (3) of Ref. [43] and also used in Ref. [42].
[50] I. M. Lifshitz, Zh. Eksp. Teor. Fiz. **42**, 1354 (1962) [Sov. Phys. JETP **15**, 939 (1962)].
[51] S. K. Chan, J. Chem. Phys. **67**, 5755 (1977).
[52] S. M. Allen and J. W. Cahn, Acta Metall. **27**, 1085 (1979).
[53] A. N. Kolmogorov, Bull. Acad. Sci. USSR, Phys. Ser. **1**, 355 (1937).
[54] W. A. Johnson and P. A. Mehl, Trans. Am. Inst. Mining Metall. Eng. **135**, 416 (1939).
[55] M. Avrami, J. Chem. Phys. **7**, 1103 (1939); **8**, 212 (1940); **9**, 177 (1941).
[56] K. Sekimoto, Phys. Lett. A **105**, 390 (1984); J. Phys. Soc. Jpn. **53**, 2545 (1984).
[57] K. Sekimoto, Physica **135A**, 328 (1986); Int. J. Mod. Phys. B **5**, 1843 (1991).
[58] E. Jordão Neves and R. H. Schonmann, Commun. Math. Phys. **137**, 209 (1991).
[59] R. H. Schonmann, Commun. Math. Phys. **147**, 231 (1992).
[60] F. Martinelli, E. Olivieri, and E. Scoppola, J. Stat. Phys. **62**, 135 (1991).
[61] E. Scoppola, J. Stat. Phys. **73**, 83 (1993).
[62] R. Kotecký and E. Olivieri, J. Stat. Phys. **70**, 1121 (1993).
[63] E. Scoppola, Physica A **194**, 271 (1993), and references cited therein.
[64] W. H. Press *et al.*, *Numerical Recipes: The Art of Scientific Computing* (Cambridge University Press, Cambridge, 1992).
[65] H. L. Richards, S. W. Sides, M. A. Novotny, and P. A. Rikvold, J. Magn. Magn. Mater. (to be published).
[66] A. B. Bortz, M. H. Kalos, and J. L. Lebowitz, J. Comput. Phys. **17**, 10 (1975).
[67] M. A. Novotny, Comp. Phys. **9**, 46 (1995).
[68] The simulated $F_0(m)$ are very smooth, as seen in Fig. 1(a). However, the residual noise combined with the high resolution in $m$ ($\Delta m=2/L^2$) made it necessary to calculate the numerical derivatives using a fourth-order Savitzky-Golay smoothing filter (subroutine SAVGOL from Ref. [64]) with a window on the order of the width of the deep, narrow minimum in $h(m)$.